Floquet theory of microwave absorption by an impurity in the two-dimensional electron gas

Alexei D. Chepelianskii
LPS, Université Paris-Sud, CNRS, UMR 8502, Orsay F-91405, France

Dima L. Shepelyansky
Laboratoire de Physique Théorique du CNRS, IRSAMC, Université de Toulouse, UPS, Toulouse 31062, France

(Received 22 November 2017; revised manuscript received 12 February 2018; published 13 March 2018)

We investigate the dynamics of a two-dimensional electron gas (2DEG) under circular polarized microwave radiation in the presence of dilute localized impurities. Inspired by recent developments on Floquet topological insulators we obtain the Floquet wave functions of this system which allow us to predict the microwave absorption and charge density responses of the electron gas; we demonstrate how these properties can be understood from the underlying semiclassical dynamics even for impurities with a size of around a magnetic length. The charge density response takes the form of a rotating charge density vortex around the impurity that can lead to a significant renormalization of the external microwave field which becomes strongly inhomogeneous on the scale of a cyclotron radius around the impurity. We show that this inhomogeneity can suppress the circular polarization dependence which is theoretically expected for microwave induced resistance oscillations but which was not observed in experiments on semiconducting 2DEGs. Our explanation for this so far unexplained polarization independence has close similarities with the Azbel'-Kaner effect in metals where the interaction length between the microwave field and conduction electrons is much smaller than the cyclotron radius due to skin effect generating harmonics of the cyclotron resonance.

DOI: 10.1103/PhysRevB.97.125415

I. INTRODUCTION

The topological properties of condensed matter systems have been the focus of intense theoretical and experimental research starting from the discovery of the quantum Hall effect [1,2]. Recently it has been suggested that some systems can develop new topological properties under external periodic driving, leading to the concept of Floquet topological insulators [3–5] and to their realization in photonic systems [6–8]. In parallel an active research on the effect of microwave irradiation of ultrahigh mobility two-dimensional systems revealed striking microwave induced resistance oscillations (MIRO) at weak nonquantizing magnetic fields [9]. These oscillations are characterized by a periodic dependence on the ratio between the microwave and cyclotron frequencies. At sufficiently high microwave power the oscillations grow in amplitude leading to the formation of zero-resistance states [10,11]. This effect has now been observed in several systems [12–16], and it has been shown that the zero-resistance regime can lead to the onset of new thermodynamic properties like an incompressible behavior usually associated with the quantum Hall effect [17]. The theoretical understanding of MIRO has attracted considerable attention stimulating several approaches. Semiclassical and quantum kinetic equation formalisms have been used to derive an analytic description for the magnetic field dependence of microwave induced oscillations due to interactions with residual impurities in the two-dimensional electron gas in a Born approximation limit where recollision or memory effects were treated perturbatively [18–22]. Classical dynamics has been used to analyze memory effects in the nonperturbative limit and to derive in a transparent manner the results from kinetic equation calculations [23,24]. These theories provide a good description of the experimental magnetic field dependencies. However they are intrinsically linked to the cyclotron resonance and share its strong dependence on the polarization of the radiation. This simulated careful polarization dependent experiments [25–29]; in particular it was shown that contrarily to cyclotron resonance MIRO is not sensitive to the orientation of circularly polarized microwave irradiation [25,28]. This disagreement stimulated the development of extrinsic theories where the influence of edges and contacts was considered as the main mechanism behind MIRO [30,31]. But recent experiments with a spatially resolved THz excitation [28,29] have confirmed the bulk origin of MIRO leaving the circularly polarized radiation dependence unexplained.

Here we address this issue by developing a Floquet description of the interaction between a local impurity and a two-dimensional electron gas (2DEG) under circularly polarized radiation. We show that the properties of quantum Floquet wave functions can be understood from classical dynamics even in the limit where the radius of the impurity is of the order of the magnetic length. We then use this theory to compute the absorbed microwave power using both quantum and semiclassical formalisms and show the appearance of a rotating redistribution of electron density around the impurity that locally enhances the external electromagnetic field. We argue that the inclusion of this screening correction suppresses the dependence on polarization chirality and discuss analogies with the cyclotron resonance oscillations in metals known as the Azbel'-Kaner effect [32,33] (see also overview of this effect in Ref. [34]).

Appearance of rare isolated impurities in 2DEG can have various origins, interface roughness, impurity atoms, or growth induced inhomogeneities [35]. There seems to be no consensus

 ©2018 American Physical Society

at the moment on the type of impurities that determine the transport time scales in ultrahigh quality samples; in our studies we thus consider a generic impurity model as a circular positive or negative potential on a radius r_d being smaller than the cyclotron radius R_c. All other scattering contributions are incorporated into an effective scattering time τ. We consider the limit of an isolated impurity; this assumption is reasonable as long as the cyclotron radius R_c is smaller than the average distance between impurities $n_i^{-1/2}$ where n_i is the density of impurities. Assuming that all the scattering originates from such localized impurities we obtain an upper bound (as other sources of scattering are present) $n_i \lesssim (\lambda_F \ell_e)^{-1}$ where we assumed that the Fermi wavelength λ_F gives the scattering cross section impurities and ℓ_e is the elastic mean free path. Taking the parameters for ultrahigh mobility sample used in Refs. [10,11] we find that the isolated impurity condition $R_c(\lambda_F \ell_e)^{-1/2} < 1$ is then met when the magnetic field B is larger than 0.03 T; if we take on the other hand high density samples [13] we find instead $B > 0.25$ T. Interestingly in both cases this calculation gives a correct estimate of the lowest magnetic field at which zero resistance states were observed in the experiments.

II. MODEL DESCRIPTION AND DYNAMICS: QUANTUM AND CLASSICAL THEORY

We consider an isolated impurity with a rotation invariant potential $V_i(r)$ embedded in a surrounding 2DEG under a magnetic field B giving rise to cyclotron motion with a frequency $\omega_c = qB/m$ and a cyclotron radius $R_c = v_F/\omega_c$ (m and q are the carrier effective mass and charge, v_F and $E_F = mv_F^2/2$ are the Fermi velocity and energy, r is the radial distance from the impurity center). A circularly polarized irradiation induces an additional time-dependent potential $V_{ac}(t) = -qE_{ac}r\cos(\theta - \omega t)$ where ω is the microwave frequency and θ is the polar angle. The system Hamiltonian is the sum of static and time-dependent contributions and reads:

$$\hat{H}(t) = \hat{H}_0 + V_i(r) - qE_{ac}r\cos(\theta - \omega t), \qquad (1)$$

where $\hat{H}_0$ is the charge kinetic energy in a magnetic field. This time dependent Hamiltonian can be analyzed using general Floquet-states theory, however as the static part of the Hamiltonian has rotational invariance it is more convenient to move first to the rotating frame where the Hamiltonian becomes stationary. This transformation is analogous to the rotating frame approximation in spin resonance or in atomic physics which becomes exact for a circularly polarized excitation. For this purpose we introduce the rotating frame angle $\theta_{\mathcal{R}} = \theta - \omega t$ and seek the solutions of the Schrödinger equation in the form $\psi = |\psi_{\mathcal{R}}(r,\theta_{\mathcal{R}})\rangle e^{-i\epsilon t/\hbar}$. The wave function $\psi_{\mathcal{R}}$ then obeys a stationary Schrödinger equation with a modified Hamiltonian $\hat{H}_{\mathcal{R}}$:

$$\hat{H}_{\mathcal{R}} = \hat{H}_0 + V_i(r) - qE_{ac}r\cos\theta_{\mathcal{R}} - \omega\hat{l}_z, \qquad (2)$$

where $\hat{l}_z$ is the orbital momentum operator defined from the position of center of the impurity; by construction it is conjugated to the phase $\theta_{\mathcal{R}}$. The eigenfunctions ψ_n of this Hamiltonian $\hat{H}_{\mathcal{R}}$ give the Floquet wave functions in the laboratory frame $\psi = \psi_n(r,\theta_{\mathcal{R}} = \theta - \omega t)$; they correspond to wave functions rotating at frequency ω. Since the rotating frame Hamiltonian is stationary it is possible to analyze the properties of the Floquet eigenstates using the technique of Wigner functions and associated Husimi representations [36] that allows us to draw a parallel between the quantum evolution and conceptually simpler classical dynamics. For example, we will show that the classical description leads to a straightforward description of the periodic dependence of transport properties on the frequency ratio $J = \omega/\omega_c$. The methods of numerical solution of the Schrödinger equation and Newton dynamics of the Hamiltonian (2) are described in the Appendix Sec. 1, Sec. 2, Sec. 3, and Sec. 4.

We note that in the rotation frame the initial time dependent Hamiltonian (1) is transformed to the stationary conservative Hamiltonian (2). The transformation is exact and simplifies the numerical studies of this system. However, the time dependent effects directly present in the initial laboratory frame play a very important role. Indeed, as we will see below, the microwave field leads to emergence of chaos and kinetic energy growth of electron in a vicinity of impurity. This energy growth is stabilized by the dissipative effects present in 2DEG. Due to these reasons the time dependent perturbation is of principal importance and this justifies the Floquet theory term used in this paper. The stationary form of the Hamiltonian (2) is rather formal since due to the possibility of unlimited positive values of orbital momentum l_z the kinetic electron energy can be arbitrary high. The use of circular polarization allows us to perform efficient numerical analysis of classical and quantum evolution being rather complicated for numerical analysis with nonlinear dynamics and many quantum levels. Within our Floquet analysis we are able to model numerically the dissipative processes of the kinetic classical theory and quantum master equation for density matrix. The progress with numerical simulations allows us to understand the nontrivial features of polarization dependence established experimentally in Refs. [25,28,29].

Figure 1(a) shows the Husimi representation of a typical eigenstate of $\hat{H}_{\mathcal{R}}$ for a hard disk potential with radius $r_d/\ell_B = 1$ (we introduce the magnetic length $\ell_B = \sqrt{\hbar/m\omega_c}$) under microwave irradiation at $J = 2.7$ and microwave excitation amplitude $qE_{ac}\ell_B/\hbar\omega_c = 0.3$. It gives the semiclassical probability density in the phase space l_z,θ_R in the vicinity of the impurity at $r \approx r_d$. It is computed by numerical diagonalization of the Hamiltonian $\hat{H}_{\mathcal{R}}$ and using the approach described in Refs. [37,38] and Appendix Sec. 2. The Husimi density highlights a resonant structure with a significant variation of orbital momentum l_z with the conjugated phase θ_R. The variation of orbital momentum is due to the action of the microwave field which spoils orbital momentum conservation existing at $E_{ac} = 0$. On top of the quantum Husimi distribution we have overlaid the corresponding Poincaré section of classical orbits [39] obtained from the classical dynamics described by $H_{\mathcal{R}}$. The results demonstrate that the resonant structure in the l_z,θ_R plane is accurately reproduced by classical dynamics even if the radius of the disk is comparable with the quantum magnetic length.

The resonant structure in phase space revealed by the Husimi distribution and associated Poincaré section can be understood by computing the change in dynamical variables after each free evolution cyclotron period and subsequent collision with the impurity. We assume that the impurity potential $V_i(r)$ vanishes outside a characteristic typical radius $r_d \ll v_F/\omega_c$ and note by α the polar angle of the velocity in

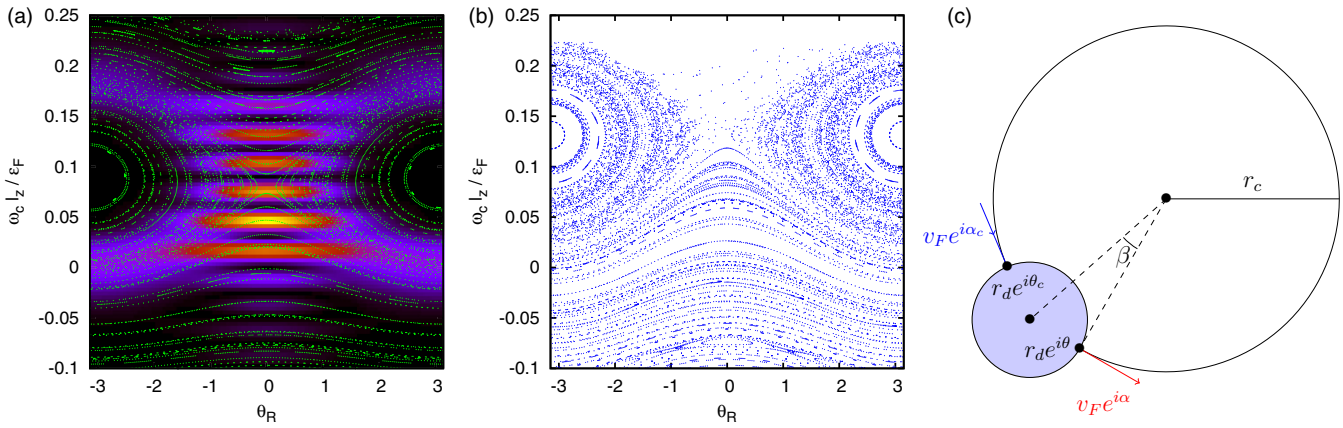

FIG. 1. Left panel (a): density of Husimi function at the disk radius $r = r_d$ shown by color (maximum for yellow/white; minimum zero for violet/black), Poincaré section for classical Hamiltonian dynamics of (2) is drawn at the moment of collision with disk and is shown by green dots; here $J = 2.7, r_d/\ell_B = 1, qE_{ac}\ell_B/\hbar\omega_c = 0.3$ at energy $\epsilon_F/\hbar\omega_c \approx 40$. Middle panel (b): classical Poincaré section of the collision map (5) at parameters of panel (a). Right panel (c): geometry of collision.

the laboratory frame when an electron leaves the interaction region $r \leqslant r_d$. The images of typical trajectory collisions with the disk can be found in Ref. [23] [see also Fig. 1(c) and Fig. 8 in Appendix]. Without microwaves the change of α to its value $\bar{\alpha}$, taken after a cyclotron orbit rotation and a recollision event with the impurity, can be expressed as

$$\bar{\alpha} = \alpha + \sigma(l_z), \tag{3}$$

where σ is a function depending on the impurity potential and on the orbital momentum giving the impact parameter with the impurity (the geometry of collision is shown in Fig. 1(c)). For a hard disk impurity $\bar{\alpha} = \alpha + 2\chi - \pi$, where $\chi = \alpha - \theta$ is the relative angle between the velocity and the impact position; χ is related to orbital momentum through $l_z = mv_F r_d \sin\chi$. A more general expression of $\sigma(l_z)$ valid for a step potential of fixed height U_i is given in Appendix Sec. 4.

Without microwaves the orbital momentum l_z and the total energy H_0 are conserved. In the presence of microwaves however $H_{\mathcal{R}}$ is the only integral of motion. The change of orbital momentum during the free-evolution time between two successive collisions can thus be expressed as:

$$\delta l_z = \frac{\delta H_0}{\omega} = \frac{1}{\omega}\int_0^{2\pi/\omega_c} q\mathbf{E}_{ac}(t)\mathbf{v}(t)dt$$
$$= \frac{qv_F E_{ac}}{\omega(\omega-\omega_c)}[\sin\alpha_R - \sin(\alpha_R - 2\pi J)], \tag{4}$$

where we introduced $\alpha_{\mathcal{R}}$ the velocity polar angle in the rotating frame $\alpha_{\mathcal{R}} = \alpha - \omega t$, $J = \omega/\omega_c$. During the short collision with the impurity we can neglect the microwave field so that in this approximation the orbital momentum is conserved in the interaction region. Combining the two previous equations we find a symplectic map [39,40] describing the evolution of the velocity polar angle $\alpha_{\mathcal{R}}$ and conjugated orbital momentum l_z from one collision to another:

$$\bar{l}_z = l_z + F[\sin\alpha_R - \sin(\alpha_R - 2\pi J)],$$
$$\bar{\alpha}_{\mathcal{R}} = \alpha_{\mathcal{R}} + \sigma(\bar{l}_z) - 2\pi J, \quad F = qv_F E_{ac}/[\omega(\omega-\omega_c)]. \tag{5}$$

Here bars mark the dynamical values of variables after one map iteration (one collision) and σ is a function describing the change in the angle of the velocity after collision with an impurity with an impact parameter given by l_z. For colliding trajectories, the orbital momentum is given by $l_z = mv_F r_d \sin\chi$ where χ is the angle between the impact position on the impurity and the impact velocity (see Appendix Sec. 4). For a hard disk potential we find $\sigma = 2\chi - \pi$ whereas for a strong attractive potential σ is π shifted and is given by $\sigma = 2\chi$. The behavior of the map then depends on the dimensionless force $\epsilon = qE_{ac}/[mr_d\omega(\omega-\omega_c)]$ which can be strong even for weak amplitudes of the microwave field since r_d appears in the denominator. More details on map derivation are presented in Appendix Sec. 4.

This map gives a good description of the dynamics leading to practically the same Poincaré section as exact Hamiltonian evolution [see Fig. 1(b)] and allows us to understand the physical origin of the oscillatory dependence on the parameter $J = \omega/\omega_c$. In the frame of the free-particle moving under magnetic and microwave fields, the microwave leads effectively to a vibration of the impurity position; the change in orbital momentum thus depends on the position of the impurity at the moment of recollisions. In the limit of a small impurity $r_d \ll R_c = v_F/\omega_c$ the time between recollisions will be given by the cyclotron period, and the position of the impurity in the vibrating frame will depend periodically on J. For integer values of J the position of the impurity does not change from collision to collision leading to a vanishing kick $\delta l_z \propto [\sin\alpha_R - \sin(\alpha_R - 2\pi J)]$ as derived in Eq. (4).

This result may seem surprising from a quantum point of view, since one could expect a strong effect of microwave at integer harmonics of the cyclotron resonance as it would to correspond to resonant absorption of photons between separated Landau levels. This issue can be elucidated through the computation of the absorbed microwave power in both quantum and semiclassical cases using the quantum Floquet master equation and classical kinetic equation and approximate map calculations. This calculation will also reveal the connection between the absorbed microwave power and an effective rotating dipole that appears due to the formation of a charge density vortex around the impurity in the rotating frame. This will then give some insight on the possible origin of the

so far unexplained circular polarization dependence in MIRO experiments.

III. MASTER AND KINETIC EQUATIONS

The Floquet eigenstates form a natural basis to write the master equation which describes excitation of the 2DEG by microwaves and relaxation to equilibrium [41,42]. As we would like to focus on the physical properties of the Floquet eigenstates around an impurity, we assume a simplified master equation in a relaxation time approximation (more sophisticated relaxation models have been studied in the limit of semiclassical quantum kinetic theory but without computing the exact Floquet states [22]). The master equation for the density matrix $\hat{\rho}(t)$ in the relaxation time approximation then reads:

$$\frac{\partial \hat{\rho}}{\partial t} = -\frac{i}{\hbar}[\hat{H}(t), \hat{\rho}] - \frac{\hat{\rho} - \hat{\rho}_{eq}}{\tau}. \tag{6}$$

The equilibrium density matrix $\hat{\rho}_{eq}$ is the equilibrium Fermi-Dirac distribution for the Hamiltonian without microwaves. Following general Floquet theory, we write this equation in the basis of the Floquet eigenstates. In our problem those are the eigenfunctions $|\psi_{\mathcal{R}}^{(n)}\rangle$ of the rotating frame Hamiltonian $\hat{H}_{\mathcal{R}}$. We find that the matrix elements $\hat{\rho}_{nm} = \langle\psi_{\mathcal{R}}^{(n)}|\hat{\rho}|\psi_{\mathcal{R}}^{(m)}\rangle$ obey the following equation:

$$\frac{\partial}{\partial t}\rho_{nm} + \frac{i}{\hbar}\epsilon_{nm}\rho_{nm} = -\frac{\rho_{nm} - \rho_{eq,nm}}{\tau}, \tag{7}$$

where $\epsilon_{nm} = \epsilon_n - \epsilon_m$ is the difference of associated quasienergies.

The quantity $\rho_{eq,nm} = \langle\psi_{\mathcal{R}}^{(n)}|\hat{\rho}_{eq}|\psi_{\mathcal{R}}^{(m)}\rangle$ can *a priori* depend on time due to the time dependence of the Floquet states $\psi_{\mathcal{R}}$. However these states are stationary in the rotating frame $\theta_{\mathcal{R}} = \theta - \omega t$ and the steady state Hamiltonian $\hat{H}_0$ is rotation invariant. Thus, as it can be shown by an explicit calculation, the matrix elements $\rho_{eq,nm}$ are actually independent of time.

At large times $t \gg \tau$, the density matrix $\hat{\rho}$ converges to a stationary solution in the rotating frame basis:

$$\rho_{nm} = \frac{\rho_{eq,nm}}{1 + \frac{i}{\hbar}\epsilon_{nm}\tau}. \tag{8}$$

This steady state density matrix can be used to compute several physical properties: microwave absorption, redistribution of charges around the impurity, induced rotating dipole appearing near the impurity due to the charge redistribution in the rotating frame.

To deepen our understanding of the link between quantum and classical dynamics, we also solve the associated kinetic Vlasov equation for the distribution function in the classical phase space:

$$\frac{\partial f}{\partial t} + \{f, H(t)\} = -\frac{f - f_{eq}}{\tau}, \tag{9}$$

where we introduced the Poisson brackets defined as

$$\{f, H\} = \frac{\partial f}{\partial \mathbf{r}}\frac{\partial H}{\partial \mathbf{p}} - \frac{\partial f}{\partial \mathbf{p}}\frac{\partial H}{\partial \mathbf{r}}. \tag{10}$$

As in the quantum case, the kinetic equation becomes time independent in the rotating frame. In the rotating frame the distribution function $f_{\mathcal{R}}$ is found numerically by integrating the characteristic equation $\frac{df_{\mathcal{R}}}{dt} = -\frac{f_{\mathcal{R}} - f_{eq}}{\tau}$ along trajectories in this frame. The details of numerical simulations of the quantum master equation and the classical kinetic equation are given in Appendix Secs. 1,3,5.

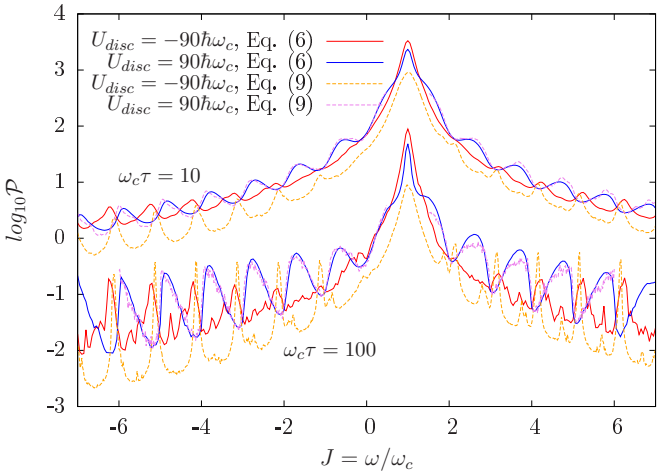

FIG. 2. Absorption power $\mathcal{P}$ (in arbitrary units) is shown as a function of $J = \omega/\omega_c$ for $r_d/\ell_B = 2$ at $qE_{ac}\ell_B/\hbar\omega_c = 0.1$ and $\epsilon_F/\hbar\omega_c = 60$. Data are shown for two relaxation times with $\omega_c\tau = 10,100$ (different signs of J correspond to different signs of circular polarization, $\omega_c\tau = 10$ and 100 datasets are vertically shifted for clarity). Quantum results are obtained from the master equation on the density matrix; they are compared with classical results from the kinetic equation. An excellent agreement between quantum and classical results is observed for a repulsive potential. For an attractive potential the agreement is only qualitative for the kinetic equation giving the same phase of microwave absorption oscillations as the quantum calculation.

IV. MICROWAVE POWER ABSORPTION BY ELECTRONS INTERACTING WITH AN IMPURITY

The microwave power absorbed by electrons interacting with an isolated impurity can be obtained by averaging the operator $\mathbf{v} \cdot q\mathbf{E}_{ac}$ in the rotating frame. In the quantum case, this is done by computing the trace: $\mathcal{P} = \mathrm{Tr}(\hat{\rho}\mathbf{v} \cdot q\mathbf{E}_{ac})$, for the Vlasov equation a similar procedure, described in Appendix, is employed.

The dependence of the absorbed power $\mathcal{P}$ on J is shown in Fig. 2 for a strongly repulsive ($U_{\mathrm{disc}} > E_F > 0$) and attractive ($U_{\mathrm{disc}} < -E_F < 0$) impurity potential; different signs of J correspond to different signs of circular polarization. The absorbed power shows a resonance at $J = 1$ which corresponds to cyclotron resonance (which appears only for the active polarization $J > 0$), $\mathcal{P}$ then decays as expected from an usual Drude model but presents additional oscillations with a period $\Delta J = 1$ which become more pronounced as $\omega_c\tau$ grows. These oscillations appear due to the periodic structure in J in Eq. (5) and correspond to MIRO like oscillations of the absorbed microwave power; they are related to consecutive collisions between an electron and impurity (memory effects) [23,24,43]. As expected at small amplitudes of microwave field the absorbed power $\mathcal{P}(J)$ is proportional to ${E_{ac}}^2$, we also checked that the envelope of the oscillations is well approximated by the classical Drude formula $\mathcal{P} =$

$(q^2/m)\tau/[1+\tau^2(\omega-\omega_c)^2]{E_{ac}}^2$ (see Fig. 13 in Appendix Sec. 6 and discussion of parameter scaling dependence given there; details of numerical computations of absorption power are given in Appendix Sec. 6). For the repulsive impurity the results of the quantum master equation and the classical kinetic theory are in quantitative agreement; the agreement is less accurate for attractive impurities but the correct peak positions are reproduced by the kinetic equation even in this case. It is likely that the quantum dynamics inside an attractive impurity has stronger deviations from the classical behavior when its depth is comparable with the Fermi energy E_F. The good overall agreement between quantum and classical simulations holds even if the impurity radius r_d is only two times larger than the magnetic length (in Appendix we show that this trend continues even for smaller r_d). An interesting property that appears in Fig. 2 is that the oscillations in microwave absorption are phase shifted between the repulsive and attractive potentials; this shift is related to the additional π contribution that appears in Eq. (5) for the attractive potential. According to this equation the change of orbital momentum due to the action of the microwave field over a cyclotron period vanishes for integer values of J. This leads to an absorption dip at integer J values with different lineshapes depending on the sign of the potential of the impurity. For a repulsive potential (at $\omega_c\tau = 100$) integer J correspond to an absorption minimum with maxima occurring close to half integer J values. For the attractive potential, the phase π shift in the map due to the interaction sign tends to move the position of the maxima near integer values which leads to a characteristic lineshape with a double peak structure centered around integer values. We note that earlier calculations of the absorbed power in the MIRO regime for the case of a repulsive potential gave similar results [43] for the position of absorption peaks/dips; Eq. (5) allows us to generalize these results to the case of an arbitrary electron/impurity interaction. We also note that the results for the absorption dependence on J obtained from the kinetic equation are also well reproduced by the symplectic map description (5) (see Fig. 9 in Appendix Sec. 5). The dependence $\mathcal{P}(J)$ is not sensitive to variation of r_d/ℓ_B as long as r_d is larger than ℓ_B; in the limit $r_d \leqslant \ell_B$ additional quantum oscillations appear around the average semiclassical absorption curve but those will probably ensemble average to zero in a macroscopic sample (see Fig. 10 in Appendix Sec. 5).

In Fig. 2 we choose to keep the cyclotron frequency ω_c constant and to vary the microwave frequency ω. This is more convenient for quantum numerical simulations since the variation of ω_c change the number of Landau levels at the Fermi energy producing additional complications. The classical results are sensitive to the ratio ω/ω_c, as well as the experimental MIRO results (see, e.g., Ref. [22]) also show the dominance of the dependence on the ration ω/ω_c. A good agreement between classical and quantum numerical simulations gives the additional justification for variation of ω with fixed ω_c.

V. CHARGE DENSITY DISTRIBUTION INDUCED BY MICROWAVE FIELD

The absorbed power $\mathcal{P}$ from the external microwave field creates a charge redistribution around an impurity. To see this it is convenient to present this power $\mathcal{P}(E_{ac})$ in the following form (see also Appendix Sec. 5):

$$\mathcal{P} = \mathrm{Tr}(\hat{\rho}\mathbf{v}\cdot q\mathbf{E}_{ac}) \approx \omega \mathrm{Tr}(\hat{\rho}\mathbf{r})\cdot(\mathbf{e}_z\times q\mathbf{E}_{ac})\,. \tag{11}$$

This formula clearly shows that in the rotating frame there is an appearance of a stationary dipole moment of charge induced by $\mathbf{E}_{ac}$. Thus in the laboratory frame we have a rotating dipole which creates a correction to the field acting on electrons.

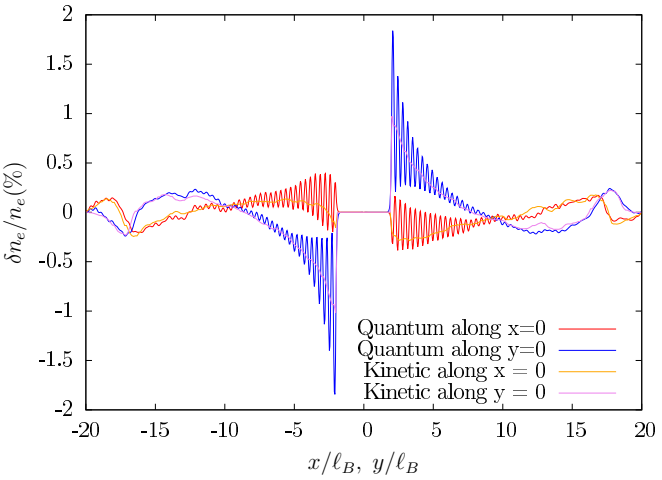

FIG. 3. Charge density $\rho(x,y)$ dependence on x (at $y=0$) and on y (at $x=0$) obtained from the quantum master equation and the classical kinetic equation presented in the rotation frame. Here the system parameters are the same as for the repulsive case in Fig. 2 with $J=2.7$ for $r_d/\ell_B = 2$ at $qE_{ac}\ell_B/\hbar\omega_c = 0.1$ and $\epsilon_F/\hbar\omega_c = 40$ with a relaxation time $\omega_c\tau = 10$.

The stationary solutions of the master equation (8) and the kinetic equation (9) allow us to compute the charge density variation induced by $\mathbf{E}_{ac}$. The charge density distribution in the presence of microwave field is shown as a function of x and y coordinates in the rotating frame in Fig. 3. In the vicinity of the impurity we have strong quantum Friedel like oscillations of density [44]. The average density lineshape from the master equation (6) calculation is well approximated by results from the classical kinetic equation (9). We note that the amplitude of density variation increases near the impurity in both cases reaching rather high values of 1–2 percent of the total electron density. The steady-state relative variation of charge density $\delta n/n_0$ in the whole (x,y) plane is shown in the rotating frame in Fig. 4 revealing the formation of a charge density vortex. Since this structure is accurately reproduced from the classical dynamics, we attribute it to a nonlinear resonance between the microwave frequency and collision frequency with the impurity which is well described by the Poincaré section of Fig. 1.

The results of Fig. 3 show that in the laboratory frame microwave driving creates a rotating charge density vortex that forms a rotating dipole moment. This dipole moment will create a rotating electric field that leads to a renormalization of the external field in the vicinity of the impurity. We now address the issue of the calculation of this renormalized field from the rotating density profiles.

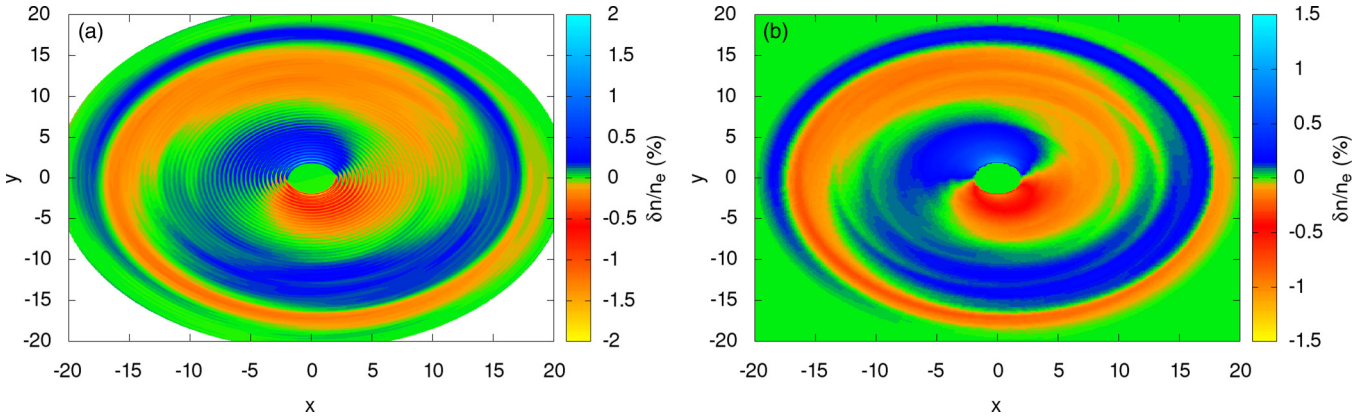

FIG. 4. Relative charge density variation $\rho(x,y) = \delta n/n_0$ (expressed in percent) shown in (x,y) plane in the rotation frame where a microwave field is directed along the x axis. Left panel shows the results of quantum simulations with the master equation; left panel show the results of the classical kinetic equation. The parameters are the same as in Fig. 3.

VI. MIRO OF SHORT RANGE FIELD NEAR IMPURITY

In the absence of screening, the rotating charge density vortex $\delta n(\mathbf{r})$ around the impurity creates an electric field that is simply given by the Coulomb integral

$$\mathbf{E}_{ee}(\mathbf{r}) = \frac{q}{4\pi\epsilon_0\epsilon_r}\int \delta n(\mathbf{r}')\frac{\mathbf{r}-\mathbf{r}'}{|\mathbf{r}-\mathbf{r}'|^3}d^2r'. \qquad (12)$$

Within a weakly-interacting electron approximation, this corresponds to a Hartree type contribution to the rescaled external field. We developed our Floquet theory for noninteracting electrons; it is thus difficult to estimate the exact form of the interaction related corrections. Qualitatively the strength of this Coulomb field may be reduced by screening from other electrons, however the characteristic length scale of the rotating charge density vortex is of the order of the cyclotron radius. A full-screening scenario seems thus unlikely as it is difficult to justify how the electron gas could provide a complete screening on this length scale at a frequency ω which is several times larger than ω_c, we thus neglect screening effects here and we present numerical results for the unscreened Coulomb integral given by Eq. (12).

To characterize the strength of the field renormalization we introduce the enhancement factor $\eta = E_{ee}/E_{ac}$, which is the ratio between the amplitude of the correction field from Eq. (12) to the amplitude of the external driving E_{ac}. The logarithm of this enhancement factor is shown in Fig. 5 on the (x,y) plane using the data for the master equation density distribution from Fig. 4. These results clearly show that the field can be enhanced by an order of magnitude in the vicinity of impurity, while far from the impurity the enhancement factor goes to zero as expected. The strongest enhancement is obtained at the boundary of the impurity and reaches two orders of magnitude.

Checking the parametric dependence of the rotating density vortex in the semiclassical model, we find that $\delta n(r)$ depends only weakly on r_d/R_c and $\omega\tau$ in a broad parameter range. This allows us to estimate the typical value of the enhancement as $\eta = E_{ee}/E_{ac} \sim q^2 n_e/(m\omega\epsilon v_F) \simeq 6$ for typical values $\omega = 2\pi \times 100$ GHz, $n_e = 3.5 \times 10^{11}$ cm^{-2}, and dielectric constant $\epsilon_d = 10\epsilon_0$. The obtained order of magnitude is consistent with the values of η in Fig. 4 at a distance of around a cyclotron radius away from the impurity, an even larger enhancement occurs at smaller distances. The estimate for η can be cast in a form that highlights its dependence on r_s the usual interaction strength parameter in 2DEG $\eta \sim r_s E_F/\hbar\omega$ [we remind that $r_s = (\pi n_e a_0^2)^{-1/2}$ where $a_0 = \frac{4\pi\epsilon_d\hbar^2}{mq^2}$ is the Bohr radius, and q is the electron charge]. A detailed discussion of scaling dependence on system parameters is given in Appendix Sec. 6 with Figs. 11–14.

The large values of the field enhancement parameter η show that a full interacting electron calculation is required to obtain consistently the field acting on the electrons. Our results suggest however the following qualitative picture: The external microwave field E_{ac} generates a strong effective circular polarized microwave field in the vicinity of the impurity which is significantly larger than the external field $E_{\rm eff} \gg E_{ac}$. This field $E_{\rm eff}$ is maximal at $r = r_d$ and decays to the external field on a typical scale $r_{\rm eff} \lesssim R_c$. It has the same circular polarization as the driving microwave field since it is created by a charge density vortex that rotates at the microwave frequency ω.

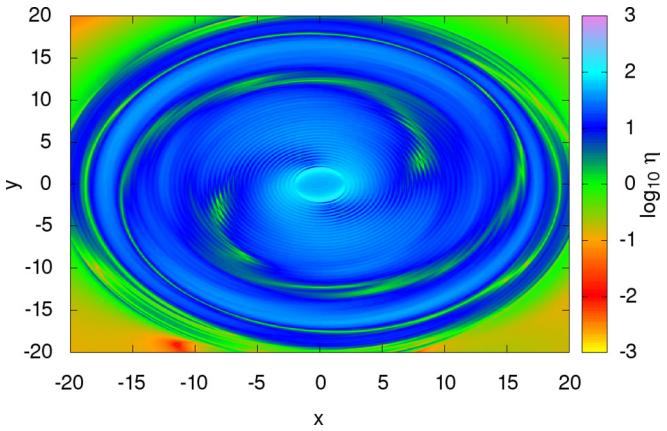

FIG. 5. Variation of the enhancement factor E_{ee}/E_{ac} of the amplitude of effective field acting on an electron due to the density variation in the (x,y) plane (see Fig. 4 left panel) induced by the external microwave field. The results, shown in the rotating frame, are obtained from the quantum master equation and the relations given by Eq. (12).

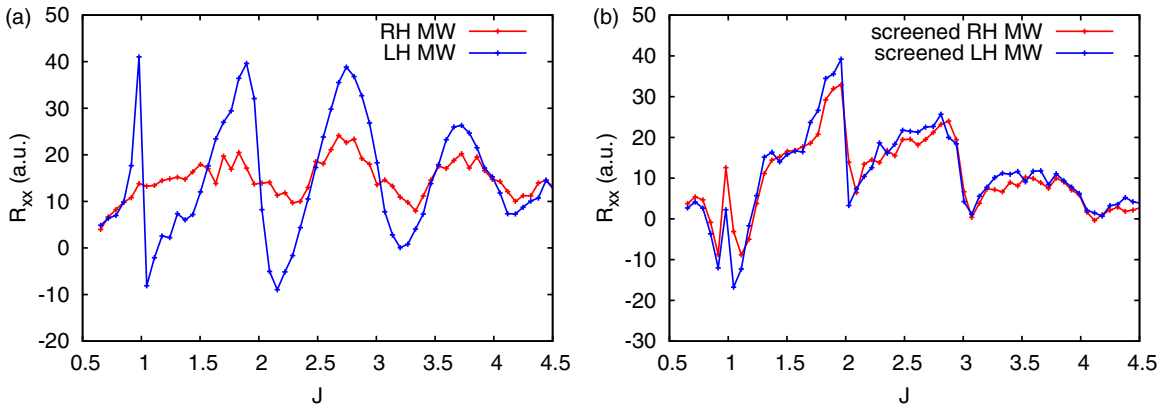

FIG. 6. Dependence of resistivity R_{xx} (in arbitrary units a.u.) on $J = \omega/\omega_c$. Left panel: the case of initial external microwave field; right panel: the case of screened renormalized field acting on a length scale $r_{\rm eff}/R_c = 0.3$. The results are obtained from the numerical simulation of classical Hamiltonian dynamics of electrons in the presence of impurities with Gaussian potential $U_{\rm amp}\exp(-r^2 r_d^{-2})$ with a density $n_i r_d^2 = 10^{-3}$, an amplitude $U_{\rm amp}/\epsilon_F = 1.5$, and a characteristic radius $r_d\omega/v_F = 0.1$. Here LH and RH correspond to left and right hand microwave (MW) polarization, respectively.

We are thus justified to consider a model where the driving microwave field is localized around the impurity instead of being homogeneous in space as considered so far in most models (with the exception of work [31] which also considered a strongly inhomogeneous field but only close to metallic contacts). We show through numerical simulations that taking into account the nonhomogeneity of the microwave field can indeed solve the puzzle of the polarization independence [25,28]. For this purpose we use the approach of Ref. [24] computing the resistivity R_{xx} for a sample of finite size with a fixed density of impurities using the Hamiltonian dynamics for electrons. The details of these simulations are given in Appendix Sec. 6.

In Fig. 6 we compare the dependence of resistivity R_{xx}, on J for the case of microwave field homogeneous in the whole space $\mathbf{E}_{ac}$ (left panel) and for the case of a model screened microwave field $\mathbf{E}_{ac}\exp(-r^2 r_{\rm eff}^{-2})$ which decays with a Gaussian profile as function of the distance from the impurity with a characteristic range $r_{\rm eff} \approx R_c/5$. The main result of these simulations is a qualitatively different dependence of R_{xx} on positive and negative J values. For a microwave field homogeneous in space there is a strong asymmetry between positive and negative circular polarization. In contrast, to a screened microwave field localized in a vicinity of impurity in a range $r_{\rm eff} \sim r_d \ll R_c$ there is no dependence of the sign of polarization (sign of J) in agreement with the experimental results reported in Refs. [25,28].

The origin of the absence of sign dependence on J for a localized field is rather simple: The range of the field is much smaller then the cyclotron radius ($r_{\rm eff} \sim r_d \ll R_c$) so that the energy change takes place only near impurity and the cyclotron resonance appearing in the kick amplitude $F \propto 1/(\omega - \omega_c)$ in (5) is absent. In fact the kick amplitude is determined only by a time interval $\Delta t_{\rm eff} = r_{\rm eff}/v_F$ of interaction of change with the field $E_{\rm eff}$ near impurity. It can be estimated as in (5) with $F \approx qE_{\rm eff}r_{\rm eff}/v_F$ being independent of the sign of polarization. In a certain sense we obtain a screened field near impurity. This situation is similar to the Azbel'-Kaner effect for cyclotron resonance absorption in metals. Due to the skin effect, the microwave field is screened in the bulk of the metal on a length scale much smaller than the cyclotron radius. The electron energy change induced by the interaction with the microwave field then takes place only in a vicinity of the metal surface [32,33]. In this case cyclotron resonance occurs not only at the cyclotron frequency but at integer harmonics (similarly to MIRO) and there is no polarization dependence since the interaction range is much smaller than the cyclotron radius.

We have shown that the rotating charge density vortex around the impurity strongly renormalizes the external microwave field since it rotates at the frequency of the external excitation. It is interesting to know if a renormalization of the static potential created by the impurity is present as well. In a mean field Hartree type approximation, such a renormalization could be created by the time averaged density profile of the rotating vortex. The time average in the laboratory frame corresponds to an average over the polar angle in the rotating frame. For the semiclassical calculation in Fig. 4(b) the charge redistribution δn_e seems antisymmetric with respect to the origin and numerical integration over angles gives a vanishing result within numerical accuracy. The situation is different in the quantum case where a closed form analytic expression for the angle averaged density can be derived (see Appendix). The time (angle) averaged density distribution $\langle\delta n_e(r)\rangle$ obtained from the quantum calculation for the parameters of Fig. 4(a) is shown in Fig. 7, while the time average value of $\langle\delta n_e(r)\rangle/n_e$ are smaller compared to the typical values for the charge density vortex they grow with microwave power. Compared to regular equilibrium Friedel oscillations that decay on the scale of the Fermi wavelength, the time averaged density profile $\langle\delta n_e(r)\rangle/n_e$ induced by microwave irradiation spreads over a much larger scale given by the cyclotron radius. In principle it is thus possible to enter a regime where the collision cross section of the impurity is mainly determined by the long range electrostatic potential created by $\langle\delta n_e(r)\rangle$ rather that by the bare short range potential of the impurity. A quantitative treatment of this scenario is beyond the scope of this paper where electron-electron interactions are not taken into account at the quantum level. In Ref. [23] we suggested an alternative scenario to the macroscopic domain formation for ZRS in semiconducting heterostructures, where the charge

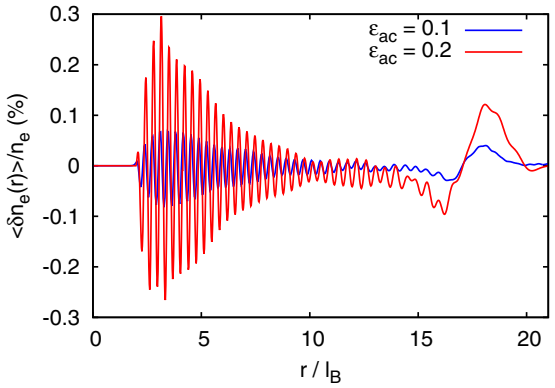

FIG. 7. Relative variation of the time averaged electron charge density $\langle \delta n_e(r) \rangle / n_e$ induced by a microwave irradiation, as a function of radial distance r from the impurity. The results are shown two microwave fields $\epsilon_{ac} = 0.1$ and 0.2 ($\epsilon_{ac} = qE_{ac}\ell_B/\hbar\omega_c$). Other parameters are as in Fig. 3 ($r_d/\ell_B = 2$, $E_F/\hbar\omega_c = 40$). $\omega_c\tau = 100$.

redistribution around an isolated sharp impurity would create a smooth cloaking potential around the impurity allowing an adiabatic passage around the impurity in which the momentum scattering would be strongly suppressed. An advantage of such a scenario compared to the more conventional macroscopic domain formation is that charges do not have to overcome macroscopic distances to create the electric field domains since the charge redistribution takes place on the scale of R_c around short range impurities. These calculations thus show that this scenario is plausible within the noninteracting electrons quantum model. We note that the experimental and theoretical results obtained in Ref. [45] also point to the importance of electron-electron interactions for the MIRO effect.

VII. DISCUSSION

We preformed extensive numerical simulations of electron dynamics in a vicinity of impurity in the presence of a circular polarized microwave irradiation. Our studies demonstrate that a description based on the classical Newton dynamics provides a good approximate description being close to the exact solution of the Schrödinger equation in the regime when the size of impurity r_d is larger than the magnetic length ℓ_B and the Fermi energy contains many quanta of cyclotron frequency ($E_F \gg \hbar\omega_c$). We also show that the classical dynamics is well described by the collision symplectic map which allows us to understand the origin of periodic dependence of MIRO on the frequency ratio $J = \omega/\omega_c$ and disappearance of microwave effect at integer J values.

The absorption power of charges in an impurity vicinity is obtained from the numerical solution of quantum master equation and the classical kinetic, or Vlasov, equation which have approximately similar average dependence on system parameters, a part of Friedel like oscillations present in the quantum case. The results obtained from the master and kinetic equations show the emergence of a strong charge redistribution created by a microwave irradiation taking the form of a rotating charge density vortex. Thus the irradiation generates a rotating dipole field localized near impurity. The strength of this induced localized field is significantly larger than the external microwave field, enhancing the external field near the impurity. This strong inhomogeneity of the microwave field results in the absence of polarization dependence and absence of the cyclotron resonance in agreement with the experimental results reported in Refs. [25,28]. This effect is similar to the Azbel'-Kaner effect [32,33] for resistance magneto-oscillation induced microwave screened in a vicinity of metal surface.

At the final stage of this work there appeared the MIRO results for electrons on a liquid helium under circularly polarized microwave excitation [46]. These experimental results show that the resistivity changes significantly with the sign of polarization in contrast to the results for 2DEG in GaAs [25,28,29] where MIRO are almost independent on the sign of the circular polarization. Since the electron densities for electrons on helium are several orders of magnitude smaller than in GaAs 2DEG, the field amplification effects discussed here are expected to be negligible. The difference in circular polarization dependence between the two systems could thus be a hint of the importance of external field renormalization in high density electron systems.

ACKNOWLEDGMENTS

We thank O. V. Zhirov for discussions and help in construction of a quantum Husimi function. A.D.C. was supported by the France ANR project SPINEX, and D.L.S. was supported in part by the Pogramme Investissements d'Avenir ANR-11-IDEX-0002-02, reference ANR-10-LABX-0037-NEXT (project THETRACOM).

APPENDIX

1. Numerical solution of quantum master equation

a. *Stationary Schrödinger equation without microwaves*

The classical Lagrangian/Hamiltonian read:

$$L = \frac{m}{2}(\dot{r}^2 + r^2\dot{\theta}^2) - \frac{m\omega_c}{2}r^2\dot{\theta} - U_w(r) \quad \text{(A1)}$$

$$H_0 = \frac{p_r^2}{2m} + \frac{1}{2mr^2}\left(p_\theta + \frac{m\omega_c r^2}{2}\right)^2 + U_w(r) \quad \text{(A2)}$$

$$= \frac{p_r^2}{2m} + \frac{p_\theta^2}{2mr^2} + \frac{\omega_c}{2}p_\theta + \frac{m\omega_c^2 r^2}{8} + U_w(r), \quad \text{(A3)}$$

where r,θ are polar coordinates, $U_w(r)$ is the impurity potential, and

$$p_\theta = mr^2\dot{\theta} - \frac{m\omega_c r^2}{2}. \quad \text{(A4)}$$

In the absence of disk potential, the angular momentum can be related with the geometrical parameters of the trajectory:

$$p_\theta = m\omega_c\frac{R_L^2 - L_c^2}{2}, \quad \text{(A5)}$$

where R_L is the Larmor radius and L_c is the distance from the guiding center to the coordinates origin.

We note that we cannot obtain the Schrödinger equation directly from quantization of this Hamiltonian; this seems due to the ill-defined nature of the operator $\hat{p}_r$ in two dimensions [47]. Instead the eigenvalue equation takes the following form which comes from rewriting the Schrödinger equation in

cylindrical coordinates [48]:

$$\hat{H}_0\psi = -\frac{\hbar^2}{2m}\left[\frac{1}{r}\frac{\partial}{\partial r}\left(r\frac{\partial\psi}{\partial r}\right)+\frac{1}{r^2}\frac{\partial^2\psi}{\partial\theta^2}\right] - \frac{i\hbar\omega_c}{2}\frac{\partial\psi}{\partial\theta}+\frac{m\omega_c^2 r^2}{8}\psi + U_w(r)\psi \quad (A6)$$

$$= E\psi. \quad (A7)$$

We introduce

$$\psi(r,\theta) = \frac{\chi(r)}{\sqrt{r}}\frac{e^{iL_z\theta}}{\sqrt{2\pi}}. \quad (A8)$$

This leads to a 1D-Schrödinger equation on $\chi(r)$:

$$-\frac{\hbar^2}{2m}\left[\frac{d^2\chi}{dr^2}+\frac{1-4L_z^2}{4r^2}\chi\right]+\frac{\hbar\omega_c L_z}{2}\chi + \frac{m\omega_c^2 r^2}{8}\chi + U_w(r)\chi = E\chi. \quad (A9)$$

We introduce dimensionless units: for length $r = x\ell_B = x\sqrt{\frac{\hbar}{m\omega_c}}$ and for energy $E = \epsilon\hbar\omega_c$. In these units

$$-\frac{1}{2}\frac{d^2\chi}{dx^2}+\frac{4L_z^2-1}{8x^2}\chi+\frac{L_z}{2}\chi+\frac{x^2}{8}\chi+U_w(x)\chi=\epsilon\chi. \quad (A10)$$

We want to express this equation as a function of the quasiclassical parameters; we thus use the relation:

$$p_\theta = m\omega_c\frac{R_L^2-L_c^2}{2} = \hbar L_z \quad (A11)$$

$$L_z = n_L(1-S^2), \quad (A12)$$

where we used $R_L = \ell_B\sqrt{2n_L}$ and introduced the parameter

$$S = \frac{L_c}{R_L}. \quad (A13)$$

The Schrödinger equation then becomes:

$$-\frac{1}{2}\frac{d^2\chi}{dx^2}+\frac{4n_L^2(1-S^2)^2-1}{8x^2}\chi+\frac{n_L(1-S^2)}{2}\chi + \frac{x^2}{8}\chi+U_w(x)\chi=\epsilon\chi, \quad (A14)$$

where n_L is the Landau level and $S = L_c/R_L$. The minimum X_m of the effective potential energy in Eq. (A10) reads $X_m^4 = 4L_z^2-1$. Using Eq. (A11) we find that collisions with the impurity (in a semiclassical approximation) occur only for orbital momenta l_z in the range:

$$l_{\min} = \frac{2n_L-\left(\sqrt{2n_L}+r_d\ell_B^{-1}\right)^2}{2} \quad (A15)$$

$$l_{\max} = \frac{2n_L-\left(\sqrt{2n_L}-r_d\ell_B^{-1}\right)^2}{2}, \quad (A16)$$

where $n_L = \epsilon_F/\hbar\omega_c$; this result is useful to estimate the range of orbital momenta that have to be included in the quantum calculation.

b. Schrödinger equation in the rotating frame

The time dependent potential for a linearly polarized field reads:

$$V_{ac} = -F_{ac}r\cos\theta\cos\omega t. \quad (A17)$$

In a circularly polarized field we find:

$$V_{ac} = -F_{ac}r\cos(\theta-\omega t) = -F_{ac}r\cos\phi, \quad (A18)$$

where $\phi = \theta-\omega t$, since the potential then depends only on ϕ we first concentrate on the circularly polarized case.

We now seek solutions of the Schrödinger equation in the rotating wave form:

$$\psi = \psi(r,\phi)e^{-iEt/\hbar}. \quad (A19)$$

The Schrödinger equation reads:

$$i\hbar\frac{d\psi}{dt} = -i\hbar\omega\frac{\partial\psi}{\partial\phi}+E\psi = \hat{H}\psi \quad (A20)$$

$$\hat{H}\psi = -\frac{\hbar^2}{2m}\left[\frac{1}{r}\frac{\partial}{\partial r}\left(r\frac{\partial\psi}{\partial r}\right)+\frac{1}{r^2}\frac{\partial^2\psi}{\partial\phi^2}\right]-\frac{i\hbar\omega_c}{2}\frac{\partial\psi}{\partial\phi} + \frac{m\omega_c^2r^2}{8}\psi + U_w(r)\psi - (F_{ac}r\cos\phi)\psi \quad (A21)$$

which has the form of a stationary Schrödinger equation. We seek the solution in the form:

$$\psi = \sum_{n,L_z} a_{n,L_z}\frac{\chi_{n,L_z}(r)}{\sqrt{r}}\frac{e^{iL_z\phi}}{\sqrt{2\pi}}e^{-iEt/\hbar}, \quad (A22)$$

where $\chi_{n,L_z}(r)$ are the eigenfunctions of the stationary part of the Hamiltonian introduced in the first section. This leads to the Schrödinger equation for a_{n,L_z}:

$$(\hbar\omega L_z+E)a_{n,L_z} = \epsilon_{n,L_z}a_{n,L_z} - \sum_{n'}[F(n,L_z;n',L_z+1)a_{n',L_z+1} + F(n,L_z;n',L_z-1)a_{n',L_z-1}], \quad (A23)$$

where we introduced the coefficients

$$F(n,L_z;n',L_z') = \frac{F}{2}\int dr\ \chi_{n,L_z}(r)\chi_{n',L_z'}(r)r. \quad (A24)$$

The transformation to the rotating frame can also be done in the classical Hamiltonian:

$$H = \frac{p_r^2}{2m}+\frac{p_\theta^2}{2mr^2}+\frac{\omega_c}{2}p_\theta+\frac{m\omega_c^2r^2}{8} + U_w(r)-F_{ac}r\cos(\theta-\omega t). \quad (A25)$$

We introduce the generating function for the canonical transformation:

$$\Phi(r,P_r,\theta,P_\phi;t) = rP_r+(\theta-\omega t)P_\phi. \quad (A26)$$

Then:

$$P_r = p_r\ ,\ \phi = \frac{\partial\Phi}{\partial P_\phi} = \theta-\omega t\ ,\ p_\theta = \frac{\partial\Phi}{\partial\theta} = P_\phi \quad (A27)$$

$$H' = H+\frac{\partial\Phi}{\partial t} \quad (A28)$$

$$= \frac{P_r^2}{2m}+\frac{P_\phi^2}{2mr^2}+\frac{\omega_c}{2}P_\phi+\frac{m\omega_c^2r^2}{8} + U_w(r)-F_{ac}r\cos\phi-\omega P_\phi \quad (A29)$$

which is consistent with the result from quantum mechanics.

c. Quantum master equation

We now consider the following master equation:

$$\frac{\partial\hat{\rho}}{\partial t} = -\frac{i}{\hbar}[\hat{H}(t),\hat{\rho}] - \frac{\hat{\rho}-\hat{\rho}_{eq}}{\tau}. \tag{A30}$$

The solution of the Schrödinger equation takes the form:

$$|\psi(t)\rangle = \psi(r,\theta-\omega t)e^{-i\epsilon t/\hbar} \tag{A31}$$

$$= |u(t)\rangle e^{-i\epsilon t/\hbar}, \tag{A32}$$

where in the last line we recognize $\psi(r,\theta-\omega t)$ as the time periodic Floquet wave function $|u(t)>$ and ϵ is the associated quasienergy. We now write the master equation in the basis of the Floquet functions

$$\begin{aligned}\left\langle u_n\left|\frac{\partial\hat{\rho}}{\partial t}\right|u_m\right\rangle &= -\frac{i}{\hbar}\left(\epsilon_n\langle u_n(t)| - i\hbar\frac{\partial}{\partial t}\langle u_n(t)|\right)\hat{\rho}|u_m\rangle \\ &+ \frac{i}{\hbar}\langle u_n(t)|\hat{\rho}\left(\epsilon_m|u_m(t)\rangle + i\hbar\frac{\partial}{\partial t}|u_m(t)\rangle\right) \\ &- \left\langle u_n\left|\frac{\hat{\rho}-\hat{\rho}_{eq}}{\tau}\right|u_m\right\rangle \end{aligned} \tag{A33}$$

$$\begin{aligned}\frac{\partial}{\partial t}(\langle u_n|\hat{\rho}|u_m\rangle) &= -i(\epsilon_n-\epsilon_m)\langle u_n|\hat{\rho}|u_m\rangle \\ &- \langle u_n|\frac{\hat{\rho}-\hat{\rho}_{eq}}{\tau}|u_m\rangle,\end{aligned} \tag{A34}$$

where we used

$$\hat{H}(t)|u_n(t)\rangle = i\hbar e^{i\epsilon_n t/\hbar}\frac{\partial}{\partial t}(|u_n(t)\rangle e^{-i\epsilon_n t/\hbar}) \tag{A35}$$

$$= \left(\epsilon_n|u_n(t)\rangle + i\hbar\frac{\partial}{\partial t}\left|u_n(t)\right\rangle\right). \tag{A36}$$

Introducing more compact notations $\rho_{nm} = \langle u_n|\hat{\rho}|u_m\rangle$, $\rho_{eq,nm}(t) = \langle u_n|\hat{\rho}_{eq}|u_m\rangle$, and $\epsilon_{nm} = \epsilon_n - \epsilon_m$, the master equation becomes:

$$\frac{\partial}{\partial t}\rho_{nm} + \frac{i}{\hbar}\epsilon_{nm}\rho_{nm} = -\frac{\rho_{nm}-\rho_{eq,nm}(t)}{\tau}. \tag{A37}$$

Writing the expression for $\rho_{eq,nm}(t)$:

$$\begin{aligned}&\rho_{eq,nm}(t) \\ &= \sum_{\epsilon_0(i,L_z)<\epsilon_F}\left(\int(dr d\theta\ r)u_n(r,\theta-\omega t)^*\frac{\chi_{i,L_z}(r)}{\sqrt{r}}\frac{e^{iL_z\theta}}{\sqrt{2\pi}}\right) \\ &\times\left(\int(dr'd\theta'\ r')u_m(r',\theta'-\omega t)\frac{\chi_{i,L_z}(r')^*}{\sqrt{r'}}\frac{e^{-iL_z\theta'}}{\sqrt{2\pi}}\right)\end{aligned} \tag{A38}$$

$$= \sum_{\epsilon_0(i,L_z)<\epsilon_F} a_{i,L_z}(n)^* a_{i,L_z}(m), \tag{A39}$$

where $a_{i,L_z}(n)$ are the projections of the Floquet wave function on the eigenstates of the unperturbed Hamiltonian which were introduced in the previous section, their expression is:

$$a_{i,L_z}(m) = \int(dr'd\theta'\ r')u_m(r',\theta'-\omega t)\frac{\chi_{i,L_z}(r')^*}{\sqrt{r'}}\frac{e^{-iL_z\theta'}}{\sqrt{2\pi}}. \tag{A40}$$

We find that $\rho_{eq,nm}(t)$ is time independent; this is a consequence of the stationary nature of the problem in the rotating frame and of the isotropic character of the equilibrium density matrix.

We thus find that in the rotating frame the density matrix converges to

$$\rho_{nm} = \frac{\rho_{eq,nm}}{1+\frac{i}{\hbar}\epsilon_{nm}\tau}. \tag{A41}$$

The charge density distribution in the rotating frame can be expressed through the density matrix

$$n_e(r,\theta_{\mathcal{R}}) = \sum_{mn} u_m^*(r,\theta_{\mathcal{R}})\rho_{mn}u_n(r,\theta_{\mathcal{R}}). \tag{A42}$$

d. Angle (time) averaged density distribution

To simplify notations we note $n_e(r) = \langle n_e(r,\theta)\rangle_\theta$ (where we have omitted the index in $\theta_{\mathcal{R}}$). We are interested in the mean electron density averaged over angles/time

$$n_e(r) = \sum_{nm}\rho_{nm}\langle u_n(r,\theta)u_m(r,\theta)^*\rangle_\theta. \tag{A43}$$

For convenience we introduce the notation:

$$U_{mn}(r) = \langle u_m(r,\theta)^* u_n(r,\theta)\rangle_\theta. \tag{A44}$$

Using the decomposition of the Floquet waves in the stationary eigenbasis we find:

$$\begin{aligned}U_{mn}(r) &= <\sum_{i,L_z} a_{i,L_z}(n)\frac{\chi_{i,L_z}(r)}{\sqrt{r}}\frac{e^{iL_z\theta}}{\sqrt{2\pi}} \\ &\times\sum_{j,L_z'} a_{j,L_z'}(m)^*\frac{\chi_{j,L_z'}(r)^*}{\sqrt{r}}\frac{e^{-iL_z'\theta}}{\sqrt{2\pi}}>_\theta\end{aligned} \tag{A45}$$

$$= \frac{1}{2\pi}\sum_{i,j;L_z} a_{j,L_z}(m)^* a_{i,L_z}(n)\frac{\chi_{j,L_z}(r)^*\chi_{i,L_z}(r)}{r}. \tag{A46}$$

With the notation

$$n_e(r) = \sum_{nm}\rho_{nm}U_{mn}(r) \tag{A47}$$

and using Eq. (A41) we find a closed form expression for the angle/time averaged density:

$$n_e(r) = \sum_{nm}\frac{U_{mn}(r)}{1+\frac{i}{\hbar}\epsilon_{nm}\tau}\sum_{\epsilon_0(i,L_z)<\epsilon_F} a_{i,L_z}(n)^* a_{i,L_z}(m). \tag{A48}$$

For a consistency check, we set $\tau = 0$ then

$$n_e(r) = \sum_{\epsilon_0(i,L_z)<\epsilon_F}\sum_{nm} a_{i,L_z}(m)U_{mn}(r)a_{i,L_z}(n)^* \tag{A49}$$

$$= \sum_{\epsilon_0(i,L_z)<\epsilon_F}\frac{1}{2\pi}\frac{|\chi_{i,L_z}(r)|^2}{r} \tag{A50}$$

due to orthogonality relations $\sum_n a_{i,L_z}(n)^* a_{j,L_z'}(n) = \delta_{ij}\delta_{L_z,L_z'}$. Another check is that we must recover the equilibrium density if there is no microwave, in this case $a_{i,L_z}(n) = \delta_{i,L_z;n}$, which leads to

$$\sum_{\epsilon_0(i,L_z)<\epsilon_F} a_{i,L_z}(n)^* a_{i,L_z}(m) = \delta_{nm} \sum_{\epsilon_0(i,L_z)<\epsilon_F} \delta_{i,L_z;n} \tag{A51}$$

$$U_{nn}(r) = \frac{1}{2\pi}\sum_{i,L_z} \delta_{i,L_z;n} \frac{|\chi_{i,L_z}(r)|^2}{r}. \tag{A52}$$

We then have:

$$n_e(r) = \sum_n U_{nn}(r) \sum_{\epsilon_0(i,L_z)<\epsilon_F} \delta_{i,L_z;n} \tag{A53}$$

$$= \sum_{\epsilon_0(i,L_z)<\epsilon_F} \frac{1}{2\pi}\frac{|\chi_{i,L_z}(r)|^2}{r}. \tag{A54}$$

The previous form is not so convenient for the efficient calculation of the dependence on r:

$$n_e(r) = \frac{1}{2\pi r}\sum_{nm}\frac{1}{1+\frac{i}{\hbar}\epsilon_{nm}\tau} \sum_{\epsilon_0(i',L_z')<\epsilon_F} a_{i',L_z'}(n)^* a_{i',L_z'}(m)$$

$$\times \sum_{i,j;L_z} a_{j,L_z}(m)^* a_{i,L_z}(n)\chi_{j,L_z}(r)^*\chi_{i,L_z}(r) \tag{A55}$$

$$n_e(r) = \frac{1}{2\pi r}\sum_{i,j,L_z} \mathcal{N}_{i,j,L_z}\chi_{j,L_z}(r)^*\chi_{i,L_z}(r), \tag{A56}$$

where

$$\mathcal{N}_{i,j,L_z} = \sum_{nm}\frac{a_{j,L_z}(m)^* a_{i,L_z}(n)}{1+\frac{i}{\hbar}\epsilon_{nm}\tau} \sum_{\epsilon_0(i',L_z')<\epsilon_F} a_{i',L_z'}(n)^* a_{i',L_z'}(m). \tag{A57}$$

e. Typical numerical parameters

We provide a complete list of the numerical parameters for the charge density vortex calculation in Fig. 4(a) from the main paper; physical parameters are $J = 2.7$, $r_d/\ell_B = 2$, $U_{\rm disc} = 90\hbar\omega_c$, $qE_{ac}\ell_B/\hbar\omega_c = 0.1$, and $\epsilon_F/\hbar\omega_c = 40$ with a relaxation time $\omega_c\tau = 10$. We select a finite set of Landau levels $n \leqslant N_L$ ($N_L = 100$) and of orbital momenta $L_{\rm min} \leqslant l_z \leqslant L_{\rm max}$ with $L_{\rm min} = -550$ and $L_{\rm max} = 650$; for all l_z in this range the one-dimensional Schrödinger Eq. (A10) is solved using a discretization with a space step (in dimensionless units) 0.02 with a total of 8000 steps. This allows us to find the N_L lowest eigenvalues $\epsilon^{(0)}_{n,l_z}$ and eigenvectors χ_{n,l_z} for each l_z. We then filter the states depending on their distance to the Fermi level selecting only states with $|\epsilon^{(0)}_{n,l_z} - \epsilon_F| < 8\hbar\omega_c$; this gives a basis with a total of 9400 states. The Schrödinger Eq. (A23) is then expressed in this basis and diagonalized using full diagonalization routines from the eigen++ packages. This allows us to find the density matrix using Eq. (A41) and the charge distribution in the rotating frame using Eq. (A42). We have checked that the numerical results are not changed when the basis is expanded to include more states in the calculation; another independent check is the good agreement we find with semiclassical calculations.

2. Husimi distribution

The Husimi function is defined via

$$H(l_z,\theta) = \sum_n \int_{-\pi}^{\pi} d\theta' e^{-(\theta-\theta'-2\pi n)^2/2} e^{il_z\theta'}\psi_{r_d}(\theta'), \tag{A58}$$

where $\psi_{r_d}(\theta')$ describes the orbital harmonics of the wave function near the disk (with radius r_d). For a hard disk potential the wave function $\psi(r,\theta)$ tends to vanish for $r \to r_d$; we have thus followed the approach of Refs. [37,38] where ψ_{r_d} is given (up to normalization) by:

$$\psi_{r_d}(\theta) = \partial_r\psi(r = r_d,\theta). \tag{A59}$$

This expression does not separate incoming and outcoming plane waves incident on the disk, an approximate separation can be achieved by defining ψ_{r_d} as:

$$\psi_{r_d}(\theta) = \sum_{n_l,l_z} a_{n_l,l_z}\frac{1}{k_{l_z,n_l}}\frac{dR_{l_Z,n_l}(r=r_d)}{dr}e^{il_z\theta}, \tag{A60}$$

where the coefficients a_{n_l,l_z} give the components of the wave function in the eigenbasis $R_{l_Z,n_l}(r)e^{il_z\theta}$ of the system without microwave field:

$$\psi(r,\theta) = \sum_{n_l,l_z} a_{n_l,l_z} R_{l_Z,n_l}(r)e^{il_z\theta} \tag{A61}$$

and gives the semiclassical momentum at the collision

$$k_{l_z,n_l} = \sqrt{2(E_{l_z,n_l} - U(l_z,r_d))/m} \tag{A62}$$

with E_{l_z,n_l} the laboratory frame energy (without microwaves) corresponding to eigenfunction $R_{l_Z,n_l}(r)e^{il_z\theta}$. We have checked that the two approaches give similar results in the limit $r_d \ll r_c$. In Fig. 1(a) we use the representation (A60) which captures the separate contribution of the ingoing wave. This can be seen from the representation of two ingoing/out-going waves $\psi(r) \propto A_k(\exp(ik(r-r_d)) - \exp(-ik(r-r_d)))$ with a certain amplitude A_k and the condition $\psi(r = r_d) = 0$.

3. Solution of the kinetic equations

The kinetic equation in the laboratory frame reads:

$$\frac{\partial f}{\partial t} + \mathbf{v}\cdot\frac{\partial f}{\partial \mathbf{r}} + \left[\omega_c\times\mathbf{v} - \frac{1}{m}\partial_r U_w + \frac{1}{m}\mathbf{F}(t)\right]\cdot\frac{\partial f}{\partial \mathbf{v}}$$

$$= -\frac{f-f_0}{\tau} \tag{A63}$$

$$\frac{\partial f}{\partial t} + \{f,H(t)\} = \frac{df}{dt} = -\frac{f-f_{eq}}{\tau}, \tag{A64}$$

where d/dt is the derivative along a trajectory in phase space. By moving to the rotating frame, the kinetic equation becomes stationary in the same way as the quantum master equation; this can be seen for example by making the canonic transform Eq. (A29) on Eq. (A64). The distribution function f thus converges to a steady state value $f(\tilde{r},\tilde{v})$ in the rotating frame coordinates $\tilde{r} = re^{-i\omega t}$ and $\tilde{v} = ve^{-i\omega t}$ (r and v are the position coordinates/velocity in the laboratory frame in the complex notation $r = x + iy$ and $v = v_x + iv_y$). We find the distribution function by integrating the equation $\frac{df}{dt} = -\frac{f-f_0}{\tau}$ along trajectories in the rotating frame.

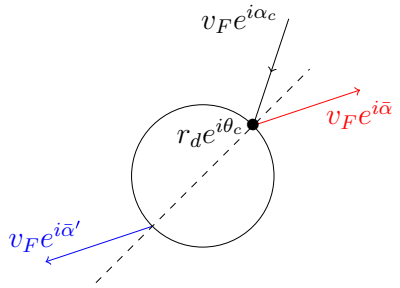

FIG. 8. Geometry of reflection during collision with a disk in case of attractive and repulsive potentials.

Trajectories outside the impurity are found by exact integration of the free equations motion in magnetic and microwave fields, they give the following expression for the change of charge velocity from $\tilde{v}_i$ at time t_i to $\tilde{v}_f$ at time t_f after a time interval $\Delta t = t_f - t_i$.

$$\tilde{v}_f = \frac{iF_{ac}}{\omega_c - \omega} + \left(\tilde{v}_i - \frac{iF_{ac}}{\omega_c - \omega}\right) e^{i(\omega_c - \omega)\Delta t} \tag{A65}$$

$$\tilde{r}_f = \tilde{r}_i e^{-i\omega\Delta t} + \frac{i\tilde{v}_i}{\omega_c} e^{-i\omega\Delta t}(1 - e^{i\omega_c\Delta t}) + F_{ac}\left(\frac{e^{-i(\omega-\omega_c)\Delta t}}{\omega_c(\omega-\omega_c)} - \frac{e^{-i\omega\Delta t}}{\omega\omega_c} - \frac{1}{\omega(\omega-\omega_c)}\right) \tag{A66}$$

The time step in the stepping algorithm is adapted as function of the distance to the impurity and collision times are found with a Newton method. For repulsive impurities a specular reflection occurs at the interface, for an attractive potential the particle is propagated inside the impurity using Eq. (A66) hold inside the impurity for a box potential.

This procedure allows us to find the distribution function for energies close to the Fermi energy on a four dimensional grid of size $N_r \times N_\theta \times N_\chi \times N_E$ where $N_r = 160$ is the number of entries for the discretization along the polar distance r, $N_\theta = 100$ the number of entries for the polar angle θ, $N_\chi = 30$ the number of entries for the angle χ between position and velocity vectors and $N_E = 30$ the number of entries for energy dicretization centered around the Fermi energy (parameters are given for calculation of Fig. 4(b) in the main text).

4. Derivation of the collision map

The geometry of elastic collision with a hard disk is shown in Fig. 1(a) and Fig. 8. The collision angles shown in these figures are defined as

$$\theta_c = 2\alpha - \theta - 2\beta + \pi$$
$$\alpha_c = \alpha + 2\pi - 2\beta, \tag{A67}$$

where

$$\beta = \arg\left(1 + i\frac{r_d}{r_c} e^{-i(\theta-\alpha)}\right). \tag{A68}$$

After the collision $r = |r|e^{i\theta}$, $v = |v|e^{i\alpha}$, $\chi = \alpha - \theta$. Without microwaves: conservation of angular momentum and energy implies that χ is conserved during a collision: $\bar{\chi} = \chi$.

New values for α can be found from geometrical arguments

$$\bar{\alpha} = \alpha + \sigma(l_z) \tag{A69}$$

$$l_z = r_d v_F \sin\chi \tag{A70}$$

$$\sigma = 2\chi - 2\arctan\left(\frac{\tan\chi}{\sqrt{1 - \frac{2U}{mv_F^2\cos^2\chi}}}\right) \tag{A71}$$

with U the amplitude of the impurity potential [$\sigma, \chi \in (-\pi/2, \pi/2)$].

In the special case of a collision with a hard disk repulsive potential ($U \to \infty$):

$$\sigma = 2\chi - \pi \tag{A72}$$

for an attractive disk potential with a large amplitude (amplitude $U \to -\infty$) this gives instead

$$\sigma = 2\chi. \tag{A73}$$

The change in kinetic energy during a period due to microwaves is

$$\bar{E} - E = \int_0^{2\pi/\omega_c} F_{ac}\mathrm{Re}(v_F e^{i\alpha_R} e^{i(\omega_c-\omega)t})dt = v_F F_{ac}\frac{\sin\alpha_R - \sin(\alpha_R - 2\pi J)}{\omega - \omega_c}, \tag{A74}$$

however

$$E \simeq H + \omega r_d\sqrt{2mH}\sin\chi, \tag{A75}$$

where $H \simeq \epsilon_F$ is conserved during the time evolution we thus find

$$\sin\bar{\chi} - \sin\chi = \frac{F_{ac}}{r_d\omega(\omega-\omega_c)}[\sin\alpha_R - \sin(\alpha_R - 2\pi J)]. \tag{A76}$$

This leads to the following map:

$$\sin\bar{\chi} = \sin\chi + \frac{F_{ac}}{r_d\omega(\omega-\omega_c)}[\sin\alpha_R - \sin(\alpha_R - 2\pi J)]$$
$$\bar{\alpha}_R = \alpha_R + 2\bar{\chi} - 2\sigma(\bar{\chi}) - 2\pi J. \tag{A77}$$

Under the approximation $\sin\chi \simeq \chi$, $\sigma(\chi) = \pi/2$ (hard disk) we recover the previous (approximate map) for $J > 0$ (check $J < 0$).

We now determine the kinetic energy from the standard map using the energy conservation in the rotating frame:

$$H = \frac{mv^2}{2} - F_{ac}R_d\cos\phi - \omega P_\phi, \tag{A78}$$

where $mv^2/2$ is the kinetic energy, ϕ the angle in the rotating frame, and P_ϕ its conjugate momentum. We need to express the rotating frame variables from the standard map variables, we find:

$$\phi = \alpha_R - \chi \tag{A79}$$

$$P_\phi = mvR_d\sin\chi - \frac{mR_d^2\omega_c}{2}. \tag{A80}$$

We thus find an equation on v:

$$H = \frac{mv^2}{2} - (m\omega R_d)v\sin\chi - F_{ac}R_d\cos\phi + \frac{mR_d^2\omega\omega_c}{2}. \tag{A81}$$

To zero order in R_d, $E = mv^2/2 = H$, going to first order in R_d we find:

$$E = H + \omega R_d\sqrt{2mH}\sin\chi + F_{ac}R_d\cos\phi \tag{A82}$$

at the Fermi energy $F_{ac}/(m\omega v_F) \ll 1$ so we can approximate:

$$E \simeq H + \omega R_d\sqrt{2mH}\sin\chi. \tag{A83}$$

The exact solution is

$$v = m\omega R_d\sin\chi + \sqrt{2H + 2F_{ac}R_d\cos(\alpha_R - \chi) + m^2R_d^2\omega^2\sin^2\chi - R_d^2\omega\omega_c}. \tag{A84}$$

We can also determine the trajectory parameters R_L, L_c:

$$R_L = \frac{1}{|\omega_c|}\sqrt{\frac{P_r^2}{m^2} + \left(\frac{P_\phi}{mr} + \frac{\omega_c r}{2}\right)^2} \tag{A85}$$

$$L_c = \frac{1}{|\omega_c|}\sqrt{\frac{P_r^2}{m^2} + \left(\frac{P_\phi}{mr} - \frac{\omega_c r}{2}\right)^2}, \tag{A86}$$

where K is the kinetic energy.

5. Calculations of absorbed microwave power

We first provide the derivation of the approximate relation between absorbed microwave power and the rotating dipole moment around the impurity.

$$\mathcal{P} = \mathrm{Tr}(\hat{\rho}\mathbf{v}\cdot q\mathbf{E}_{ac}) \tag{A87}$$

$$= -\frac{i}{\hbar}\mathrm{Tr}(\hat{\rho}[\mathbf{r},\hat{H}_0]\cdot q\mathbf{E}_{ac}) \tag{A88}$$

$$= -\frac{i}{\hbar}\mathrm{Tr}(\hat{\rho}[\mathbf{r},\hat{H}_{\mathcal{R}} + \omega\hat{l}_z]\cdot q\mathbf{E}_{ac}) \tag{A89}$$

$$= -\frac{i}{\hbar}\mathrm{Tr}(\hat{\rho}[\mathbf{r},\omega\hat{l}_z]\cdot q\mathbf{E}_{ac}) + \frac{i}{\hbar}\mathrm{Tr}(\mathbf{r}[\hat{\rho},\hat{H}_{\mathcal{R}}]\cdot q\mathbf{E}_{ac}) \tag{A90}$$

$$= \omega\mathrm{Tr}(\hat{\rho}\mathbf{r})\cdot(\mathbf{e}_z\times q\mathbf{E}_{ac}) + O(1/\tau)\,. \tag{A91}$$

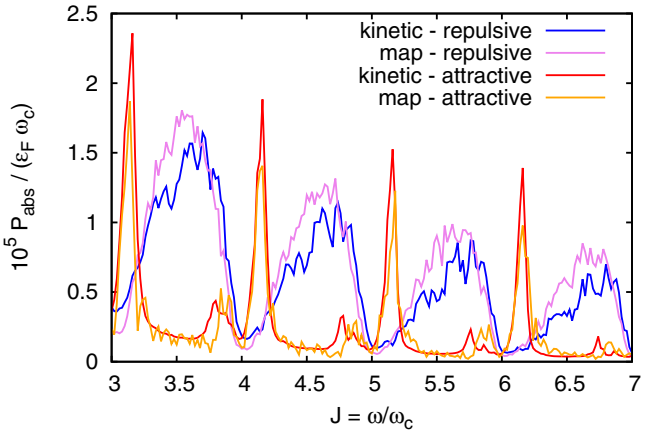

FIG. 9. Dependence of the average absorbed microwave power P_{abs} for electrons colliding with an impurity for parameters: $qE_{ac}/(m\omega v_F) = 0.013$, $r_d/R_c = 0.13$, $\omega_c\tau = 100$, $U_{\mathrm{disc}} = \pm 2\epsilon_F$, a good agreement is observed between results from the kinetic equation and from the collision map (A77).

In numerical quantum master equation calculations the power was estimated using

$$\mathcal{P} = -q\mathbf{E}_{ac}\cdot\frac{i}{\hbar}\mathrm{Tr}(\hat{\rho}[\mathbf{r},\hat{H}_0]); \tag{A92}$$

for high values of $\omega_c\tau$ we found a good agreement between exact calculations using Eq. (A92) and estimations from the dipole moment Eq. (A91).

For the semiclassical kinetic equation we can compute the average absorbed power using the relation:

$$\mathcal{P} = \left\langle\int d^2\mathbf{v}\int d^2\mathbf{r}[H_0(\mathbf{v},\mathbf{r}) - E_F]\frac{f(\mathbf{r},\mathbf{v},t) - f_0(\mathbf{r},\mathbf{v})}{\tau}\right\rangle_t \tag{A93}$$

$$= \left\langle\int d^2\mathbf{v}\int d^2\mathbf{r}\left[\frac{m\mathbf{v}^2}{2} + U_w(\mathbf{r})\right]\frac{f(\mathbf{r},\mathbf{v},t) - f_0(\mathbf{r},\mathbf{v})}{\tau}\right\rangle_t \tag{A94}$$

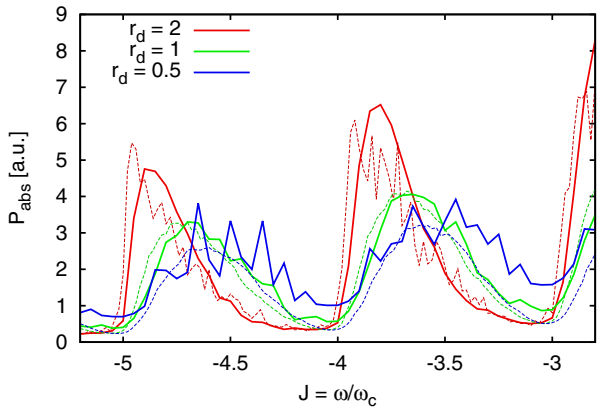

FIG. 10. Dependence of the microwave absorption $\mathcal{P}_{\mathrm{abs}}$ on J (arbitrary units) for different values of impurity radius r_d obtained from the quantum master equation Eq. (A92) (full curves) and the classical kinetic equation Eq. (A93) (dashed curves). Here $U_{\mathrm{disc}} = 2\epsilon_F$, $qE_{ac}\ell_B/\hbar\omega_c = 0.1$ and $\omega_c\tau = 100$. The semiclassical curves reproduce correctly the results from the quantum master equation. For $r_d/\ell_B = 0.5$ additional fluctuations appear in the quantum calculation around an average lineshape which is still well described by the semiclassical calculation. We attribute those to interference effects which become more pronounced when the size of the impurity becomes closer to the Fermi wavelength. In a real sample such fluctuations would probably be suppressed by ensemble average leaving only an average value which would correspond to the semiclassical result.

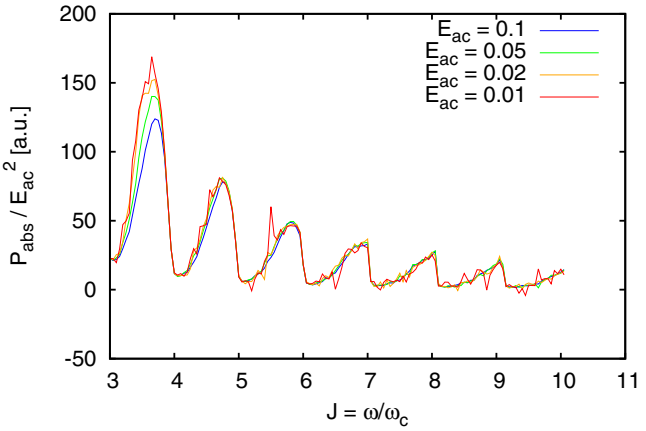

FIG. 11. Scaling dependence of the microwave absorption $\mathcal{P}_{\rm abs}$ rescaled by incident microwave power $\propto E_{ac}^2$ on J (arbitrary units) for different amplitudes of microwave field E_{ac}. The results are obtained from the quantum master equation Eq. (A92) for a repulsive impurity potential ($U_d = 90\hbar\omega_c$) at $\omega_c\tau = 100$ and $0.01 \leqslant E_{ac} \leqslant 0.1$. The data show that the scaling $P_{\rm abs} \propto E_{ac}^2$ is highly accurate. At the lowest microwave powers the data become more noisy and start to show individual resonances; we think that the sharp peaks come from contributions of individual levels trapped around the impurity that lead to sharp resonances due to the high $\omega_c\tau = 100$ value. At higher microwave power the individual resonances are broadened giving the semiclassical absorption curve.

$$= -\left\langle \int d^2\mathbf{v} \int d^2\mathbf{r} \left[\frac{m\mathbf{v}^2}{2} + U_w(\mathbf{r})\right] \frac{df}{dt} \right\rangle_t \tag{A95}$$

$$= \left\langle \int d^2\mathbf{v} \int d^2\mathbf{r} \frac{d}{dt}\left[\frac{m\mathbf{v}^2}{2} + U_w(\mathbf{r})\right] f \right\rangle_t \tag{A96}$$

$$= \left\langle \int d^2\mathbf{v} \int d^2\mathbf{r} [\mathbf{v}\cdot\mathbf{F}(t)] f \right\rangle_t, \tag{A97}$$

where H_0 is the Hamiltonian without microwaves. The advantage of equation Eq. (A93) is that the function that is integrated is always positive as opposed to Eq. (A97) which has

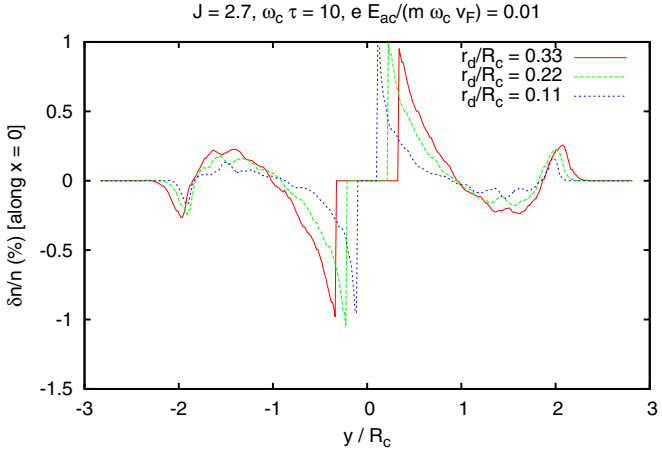

FIG. 12. Dependence of $\delta n_e(x = 0, y)/n_e$ on y/R_c for different impurity diameters, results are shown for the kinetic equation calculation.

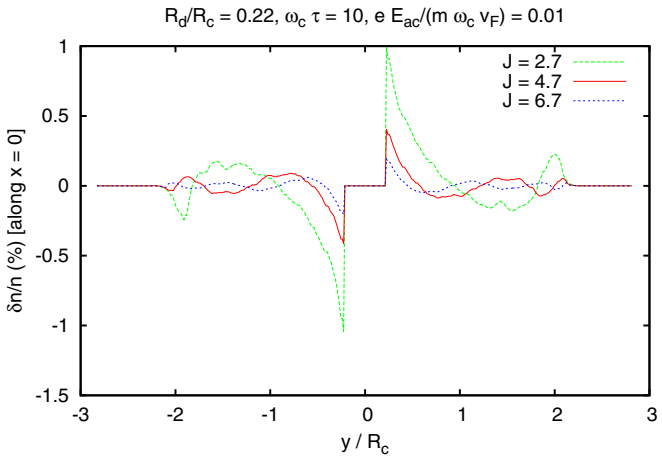

FIG. 13. Dependence of $\delta n_e(x = 0, y)/n_e$ on y/R_c for different values of $J = \omega/\omega_c$.

cancellations between positive and negative terms; Eq. (A93) is thus more suited to Monte-Carlo type of evaluation.

Finally it is possible to estimate the absorbed power from the standard map Eq. (A77), in this case the exact dynamics over one period is replaced by the approximate map; the distribution function is then computed by integrating $\frac{df}{dt} = -\frac{f - f_{eq}}{\tau}$ for free evolution with the map parameters during time $2\pi/\omega_c$ which separates successive collision events (in the approximation $r_d \ll R_c$). The absorbed power is then also computed from Eq. (A92). The results presented in Fig. 9 show that the absorbed power obtained from the kinetic equation is in good agreement with the results based on the approximate collision map Eq. (A77). This shows how physically relevant quantities can be computed from the simplified map dynamics. We note the significant difference between the case of attractive and repulsive impurity potentials.

The dependence $\mathcal{P}(J)$ at various sizes of repulsive impurity potential r_d is shown in Fig. 10. These data show good agreement between the quantum and classical simulations until the impurity diameter $2r_d$ remains larger than the magnetic length ℓ_B.

The results obtained from the quantum master equation (6) show that at small microwave driving the absorption power scales as $\mathcal{P} \propto {E_{ac}}^2$ (see Fig. 11). The results of numerical simulations of classical kinetic equation give the same scaling.

6. Estimates for charge density variation

In general we can write the following scaling form for the charge density vortex:

$$\frac{\delta n_e}{n_e} = f_7\left(xR_c^{-1}, yR_c^{-1}, r_d R_c^{-1}, \frac{qE_{ac}}{m\omega_c v_F}, \frac{\omega}{\omega_c}, \omega_c\tau, \frac{\epsilon_F}{\hbar\omega_c}\right), \tag{A98}$$

where f_7 is a dimensionless function of its seven dimensionless arguments. In the semiclassical limit the parameter $\frac{\epsilon_F}{\hbar\omega_c}$ is not relevant; this parameter describes the amplitude of microwave induced Friedel oscillations. Also in the linear response regime $\frac{\delta n_e}{n_e} \propto \frac{qE_{ac}}{m\omega_c v_F}$ (due to the connection between the rotating dipole and microwave power absorption this scaling is related to

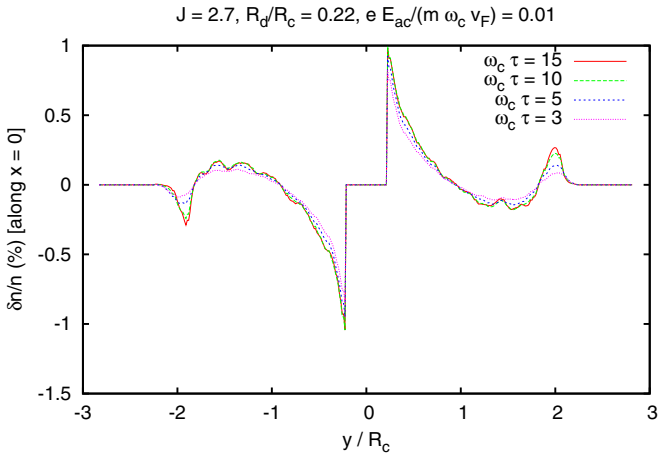

FIG. 14. Dependence of $\delta n_e(x=0,y)/n_e$ on y/R_c for different values of $\omega_c\tau$.

the $\propto E_{ac}^2$ scaling for the absorbed power, its accuracy is shown in Fig. 11). This leads to the following scaling form:

$$\frac{\delta n_e}{n_e} = \frac{qE_{ac}}{m\omega_c v_F} f_5\left(xR_c^{-1}, yR_c^{-1}, r_d R_c^{-1}, \frac{\omega}{\omega_c}, \omega_c\tau\right), \quad \text{(A99)}$$

where f_5 is a dimensionless function of the remaining five arguments.

Figures 12–14 show the scaling dependence on the remaining parameters $r_d R_c^{-1}$, $\frac{\omega}{\omega_c}$, and $\omega_c\tau$. Figure 12 shows that δn_e only weakly depends on $r_d R_c^{-1}$; this is perhaps the most surprising result since the number of electrons colliding with a given impurity during a cyclotron period is $\sim n_e R_c r_d$, this would suggest that $\delta n_e \propto n_e R_c r_d$. Our simulations show that at least in the semiclassical limit, this argument does not hold when the map parameter is small $\epsilon = \frac{qE_{ac}}{r_d\omega(\omega-\omega_c)} \ll 1$ [see Eq. (A77)]; in this case it seems that the $\propto r_d^{-1}$ dependence from the kick amplitude in the standard map equations partially cancels the $\propto r_d$ dependence from the collision cross section. Of course in the limit $r_d \to 0$ the map parameter ϵ diverges so that this cancellation holds only for sufficiently small excitation field E_{ac}. Other figures show an approximate $1/J$ dependence (for a fixed value of $\mathrm{mod}_1 J$) in Fig. 13 and a weak dependence on $\omega_c\tau$ in Fig. 14. Combining these results together we find the following scaling relation:

$$\frac{\delta n_e}{n_e} = \frac{qE_{ac}}{m\omega v_F} f_2\left(xR_c^{-1}, yR_c^{-1}\right) \quad \text{(A100)}$$

which is the result given in the main text.

[1] K. von Klitzing, G. Dorda, and M. Pepper, New Method for High-Accuracy Determination of the Fine-Structure Constant Based on Quantized Hall Resistance, Phys. Rev. Lett. **45**, 494 (1980).

[2] D. C. Tsui, H. L. Stormer, and A. C. Gossard, Two-Dimensional Magnetotransport in the Extreme Quantum Limit, Phys. Rev. Lett. **48**, 1559 (1982).

[3] T. Kitagawa, E. Berg, M. Rudner, and E. Demler, Topological characterization of periodically driven quantum systems, Phys. Rev. B **82**, 235114 (2010).

[4] N. H. Lindner, G. Refael, and V. Galitski, Floquet topological insulator in semiconductor quantum wells, Nat. Phys. **7**, 490 (2011).

[5] D. Carpentier, P. Delplace, M. Fruchart, and K. Gawdzki, Topological Index for Periodically Driven Time-Reversal Invariant 2D Systems, Phys. Rev. Lett. **114**, 106806 (2015).

[6] M. C. Rechtsman, J. M. Zeuner, Y. Plotnik, Y. Lumer, D. Podolsky, F. Dreisow, S. Nolte, M. Segev, and A. Szameit, Photonic Floquet topological insulators, Nature (London) **496**, 196 (2013).

[7] Y. H. Wang, H. Steinberg, P. Jarillo-Herrero, and N. Gedik, Observation of Floquet-Bloch states on the surface of a topological insulator, Science **342**, 453 (2013).

[8] S. Weimann, M. Kremer, Y. Plotnik, Y. Lumer, S. Nolte, K. G. Makris, M. Segev, M. C. Rechtsman, and A. Szameit, Topologically protected bound states in photonic parity-time-symmetric crystals, Nat. Mater. **16**, 433 (2017).

[9] M. A. Zudov, R. R. Du, J. A. Simmons, and J. L. Reno, Shubnikov–de Haas-like oscillations in millimeterwave photoconductivity in a high-mobility two-dimensional electron gas, Phys. Rev. B **64**, 201311(R) (2001).

[10] R. G. Mani, J. H. Smet, K. von Klitzing, V. Narayanamurti, W. B. Johnson, and V. Umansky, Zero-resistance states induced by electromagnetic-wave excitation in GaAs/AlGaAs heterostructures, Nature (London) **420**, 646 (2002).

[11] M. A. Zudov, R. R. Du, L. N. Pfeiffer, and K. W. West, Evidence for a New Dissipationless Effect in 2D Electronic Transport, Phys. Rev. Lett. **90**, 046807 (2003).

[12] D. Konstantinov and K. Kono, Novel Radiation-Induced Magnetoresistance Oscillations in a Nondegenerate Two-Dimensional Electron System on Liquid Helium, Phys. Rev. Lett. **103**, 266808 (2009).

[13] A. A. Bykov, Microwave-induced magnetic field state with zero conductivity in GaAs/AlAs Corbino disks and hall bars, JETP Lett. **87**, 551 (2008).

[14] M. A. Zudov, O. A. Mironov, Q. A. Ebner, P. D. Martin, Q. Shi, and D. R. Leadley, Observation of microwave-induced resistance oscillations in a high-mobility two-dimensional hole gas in a strained Ge/SiGe quantum well, Phys. Rev. B **89**, 125401 (2014).

[15] D. F. Kärcher, A. V. Shchepetilnikov, Yu. A. Nefyodov, J. Falson, I. A. Dmitriev, Y. Kozuka, D. Maryenko, A. Tsukazaki, S. I. Dorozhkin, I. V. Kukushkin, M. Kawasaki, and J. H. Smet, Observation of microwave induced resistance and photovoltage oscillations in MgZnO/ZnO heterostructures, Phys. Rev. B **93**, 041410(R) (2016).

[16] R. Yamashiro, L. V. Abdurakhimov, A. O. Badrutdinov, Yu. P. Monarkha, and D. Konstantinov, Photoconductivity Response at Cyclotron-Resonance Harmonics in a Nondegenerate Two-Dimensional Electron Gas on Liquid Helium, Phys. Rev. Lett. **115**, 256802 (2015).

[17] A. D. Chepelianskii, M. Watanabe, K. Nasyedkin, K. Kono, and D. Konstantinov, An incompressible state of a photo-excited electron gas, Nat. Commun. **6**, 7210 (2015).

[18] V. I. Ryzhii, Microwave-induced anisotropy of conductivity of semiconductors in quantizing magnetic fields, Sov. Phys. Solid State **11**, 2078 (1970).

[19] A. C. Durst, S. Sachdev, N. Read, and S. M. Girvin, Radiation-Induced Magnetoresistance Oscillations in a 2D Electron Gas, Phys. Rev. Lett. **91**, 086803 (2003).

[20] I. A. Dmitriev, M. G. Vavilov, I. L. Aleiner, A. D. Mirlin, and D. G. Polyakov, Theory of microwave-induced oscillations in the magnetoconductivity of a two-dimensional electron gas, Phys. Rev. B **71**, 115316 (2005).

[21] I. A. Dmitriev, A. D. Mirlin, and D. G. Polyakov, Theory of Fractional Microwave-Induced Resistance Oscillations, Phys. Rev. Lett. **99**, 206805 (2007).

[22] I. A. Dmitriev, A. D. Mirlin, D. G. Polyakov, and M. A. Zudov, Nonequilibrium phenomena in high Landau levels, Rev. Mod. Phys. **84**, 1709 (2012).

[23] O. V. Zhirov, A. D. Chepelianskii, and D. L. Shepelyansky, Towards a synchronization theory of microwave-induced zero-resistance states, Phys. Rev. B **88**, 035410 (2013).

[24] Y. M. Beltukov and M. I. Dyakonov, Microwave-Induced Resistance Oscillations as a Classical Memory Effect, Phys. Rev. Lett. **116**, 176801 (2016).

[25] J. H. Smet, B. Gorshunov, C. Jiang, L. Pfeiffer, K. West, V. Umanksy, M. Dressel, R. Meisels, F. Kuchar, and K. von Klitzing, Circular-Polarization-Dependent Study of the Microwave Photoconductivity in a Two-Dimensional Electron System, Phys. Rev. Lett. **95**, 116804 (2005).

[26] R. G. Mani, A. N. Ramanayak, and W. Wegscheider, Observation of linear-polarization-sensitivity in the microwave-radiation-induced magnetoresistance oscillations, Phys. Rev. B **84**, 085308 (2011).

[27] A. N. Ramanayaka, R. G. Mani, J. Inarrea, and W. Wegscheider, Effect of rotation of the polarization of linearly polarized microwaves on the radiation-induced magnetoresistance oscillations, Phys. Rev. B **85**, 205315 (2012).

[28] T. Herrmann, I. A. Dmitriev, D. A. Kozlov, M. Schneider, B. Jentzsch, Z. D. Kvon, P. Olbrich, V. V. Bel'kov, A. Bayer, D. Schuh, D. Bougeard, T. Kuczmik, M. Oltscher, D. Weiss, and S. D. Ganichev, Analog of microwave-induced resistance oscillations induced in GaAs heterostructures by terahertz radiation, Phys. Rev. B **94**, 081301(R) (2016).

[29] T. Herrmann, Z. D. Kvon, I. A. Dmitriev, D. A. Kozlov, B. Jentzsch, M. Schneider, L. Schell, V. V. Bel'kov, A. Bayer, D. Schuh, D. Bougeard, T. Kuczmik, M. Oltscher, D. Weiss, and S. D. Ganichev, Magnetoresistance oscillations induced by high-intensity terahertz radiation, Phys. Rev. B **96**, 115449 (2017).

[30] A. D. Chepelianskii and D. L. Shepelyansky, Microwave stabilization of edge transport and zero-resistance states, Phys. Rev. B **80**, 241308(R) (2009).

[31] S. A. Mikhailov, Theory of microwave-induced zero-resistance states in two-dimensional electron systems, Phys. Rev. B **83**, 155303 (2011).

[32] E. A. Kaner and M. I. Azbel', Theory of cyclotron resonance in metals, Sov. Phys. JETP **6**, 1126 (1958); J. Exp. Theoret. Phys. USSR **33**, 1461 (1957).

[33] M. Y. Azbel' and E. A. Kaner, Cyclotron resonance in metals, J. Phys. Chem. Solids (Pergamon Press) **6**, 113 (1958).

[34] C. Kittel, *Quantum Theory of Solids* (Wiley, New York, 1963).

[35] L. Bockhorn, I. V. Gornyi, D. Schuh, C. Reichl, W. Wegscheider, and R. J. Haug, Magnetoresistance induced by rare strong scatterers in a high-mobility two-dimensional electron gas, Phys. Rev. B **90**, 165434 (2014).

[36] F. Haake, *Quantum Signatures of Chaos* (Springer-Verlag, Berlin, 2001).

[37] B. Crespi, G. Perez, and S.-J. Chang, Quantum Poincaré sections for two-dimensional billiards, Phys. Rev. E **47**, 986 (1993).

[38] M. Hentschel, H. Schomerus, and R. Schubert, Husimi functions at dielectric interfaces: Inside-outside duality for optical systems and beyond, Europhys. Lett. **62**, 636 (2003).

[39] A. Lichtenberg and M. Lieberman, *Regular and Chaotic Dynamics* (Springer-Verlag, New York, 1992).

[40] B. V. Chirikov, A universal instability of many-dimensional oscillator systems, Phys. Rep. **52**, 263 (1979).

[41] S. Kohler. L. Jörg, and P. Hänggi, Driven quantum transport on the nanoscale, Phys. Rep. **406**, 379 (2005).

[42] M. Grifoni and P. Hänggi, Driven quantum tunneling, Phys. Rep. **304**, 229 (1998).

[43] I. A. Dmitriev, A. D. Mirlin, and D. G. Polyakov, Oscillatory ac conductivity and photoconductivity of a two-dimensional electron gas: Quasiclassical transport beyond the Boltzmann equation, Phys. Rev. B **70**, 165305 (2004).

[44] J. Friedel, Metallic alloys, J. Nuovo Cimento **7**, 287 (1958).

[45] Q. Zhang, T. Arikawa, E. Kato, J. L. Reno, W. Pan, J. D. Watson, M. J. Manfra, M. A. Zudov, M. Tokman, M. Erukhimova, A. Belyanin, and J. Kono, Superradiant Decay of Cyclotron Resonance of Two-Dimensional Electron Gases, Phys. Rev. Lett. **113**, 047601 (2014).

[46] A. A. Zadorozhko, Yu. P. Monarkha, and D. Konstantinov, Circular-Polarization-Dependent Study of Microwave-Induced Conductivity Oscillations in a Two-Dimensional Electron Gas on Liquid Helium, Phys. Rev. Lett. **120**, 046802 (2018).

[47] G. Paz, On the connection between the radial momentum operator and the Hamiltonian in n-dimensions, Eur. J. Phys. **22**, 337 (2001).

[48] L. Landau and E. Lifshitz, *Quantum mechanics: Non-Relativistic Theory* (Pergamon Press, NY, 1965).